Interest of novel N-alkylpyridinium-indolizine hybrids in the field of Alzheimer's disease: Synthesis, characterization and evaluation of antioxidant activity, cholinesterase inhibition, and amyloid fibrillation interference

Isabelle Baussanne, Olga Firstovaa, Andreea Botezatu Dediu, Camille Larosa, Bianca Furdui, Ioana Ottilia Ghinea, Aline Thomas, Sabine Chierici, Rodica Dinica, Martine Demeunynck

Interest of novel *N*-alkylpyridinium-indolizine hybrids in the field of Alzheimer's disease: synthesis, characterization and evaluation of antioxidant activity, cholinesterase inhibition, and amyloid fibrillation interference

Isabelle Baussanne,[a] Olga Firstova,[a,b] Andreea Botezatu Dediu,[c] Camille Larosa,[b] Bianca Furdui,[c] Ioana Ottilia Ghinea,[c] Aline Thomas,[a] Sabine Chierici,*[b] Rodica Dinica,*[c] Martine Demeunynck[a]

[a]*Univ. Grenoble Alpes, CNRS, DPM, Grenoble, France*
[b]*Univ. Grenoble Alpes, CNRS, DCM, Grenoble, France: e-mail: sabine.chierici@univ-grenoble-alpes.fr*
[c]*Dunarea de Jos University of Galaţi, Faculty of Science and Environment, 111 Domneasca Street, 800201, Galaţi, phone: 0336 130 251, fax: 0336 130 285, e-mail: rodinica@ugal.ro*

Keywords: indolizine-pyridinium, Alzheimer's disease, cholinesterase inhibition, amyloid fibrillation, antioxidant activity

Abstract
A small library of molecules combining indolizine and *N*-alkyl pyridinium was synthesized and evaluated in a multi-target-directed-ligand strategy for Alzheimer's disease (AD) treatment. The new compounds were classified in three series depending on the number of methylene residues linking the two heterocycles (**Ind-PyCx** with x = 0, 2 or 3). The molecules were synthesized from the corresponding bis-pyridines by two-step formation of the indolizine core including mono-alkylation of pyridine and 1,3-dipolar cycloaddition with an alkylpropiolate. Their activities against AD's key-targets were evaluated *in vitro*: acetyl- and butyrylcholinesterase (AChE and BChE) inhibition, antioxidant properties and inhibition of amyloid fibril formation. None of the three series showed significant activities against all the targets. The **Ind-PyC2** and **Ind-PyC3** series are active on eeAChE and hAChE (µM IC_{50} values). Most of the positively charged molecules from these two series also appeared active against eqBChE, however they lost their activity on hBChE. Comparative molecular modeling of **13** and **15** docked in hAChE and hBChE highlighted the importance of the substituent (*p*-methoxybenzoyl or methyloxycarbonyl, respectively) located on the indolizine C-3 for the binding. The larger molecule **13** fits more tightly at the active site of the two enzymes than **15** that shows a larger degree of freedom. The **Ind-PyC2** and **Ind-PyC3** hybrids displayed some antioxidant activity when tested at 750 µg/mL (up to 95% inhibition of DPPH radical scavenging for **10**). In both series, most hybrids were also able to interact with amyloid fibers, even if the inhibitory effect was observed at a high 100 µM concentration. The **Ind-PyC0** molecules stand out completely due to their spectroscopic properties which prevent their evaluation by Ellman's and ThT assays. However, these molecules showed interesting features in the presence of preformed fibers. In particular, the strong increase in fluorescence of **3** in the presence of amyloid fibers is very promising for its use as a fibrillation fluorescent reporter dye.

1. Introduction

The Alzheimer disease (AD) is a multifactorial neurodegenerative pathology characterized by oxidative stress and inflammatory processes, deposition of senile plaques and neurofibrillary tangles, not to forget the choline deficit due to neuron degeneration [1].

Up to now, acetylcholinesterase (AChE) inhibitors are the only molecules that have entered the clinic [2], however these drugs only delay the AD progression by increasing the local acetylcholine level. In recent years the interest for these drugs has been questioned due to the existence of side-effects and lack of proven long-term efficiency. Cholinesterase (ChE) inhibitors targeting AChE and/or BChE (butyrylcholinesterase) remain the paradigm in the search of new drugs [3]. In an effort to improve the effectiveness of these treatments and considering the complexity of AD, the multi-target-directed ligands (MTDL) approach has gained a growing importance [4-8]. Two or three AD-related features were simultaneously targeted by designing molecules that conjugate ChE inhibition with other properties, such as antioxidant or β-amyloid anti-aggregation activities. In a commonly used approach, heterodimers were prepared by linking a known AChE inhibitor to a molecule aimed to a different activity or biological target [9, 10]. A wide variety of such hybrids have been prepared as recently reviewed [11], including pyridinium containing hybrids [12-19].

Our groups have been involved for several years in the synthesis and study of the physical, chemical and biological properties of heterocyclic compounds made of pyridinium salts and indolizines. Both heterocycles possess a wide variety of interesting properties [20-23] (for examples of active molecules, see Figure 1). It is worth highlighting the fluorescence properties of the indolizine nucleus which has been used in the design of fluorescent tags or markers [24-30].

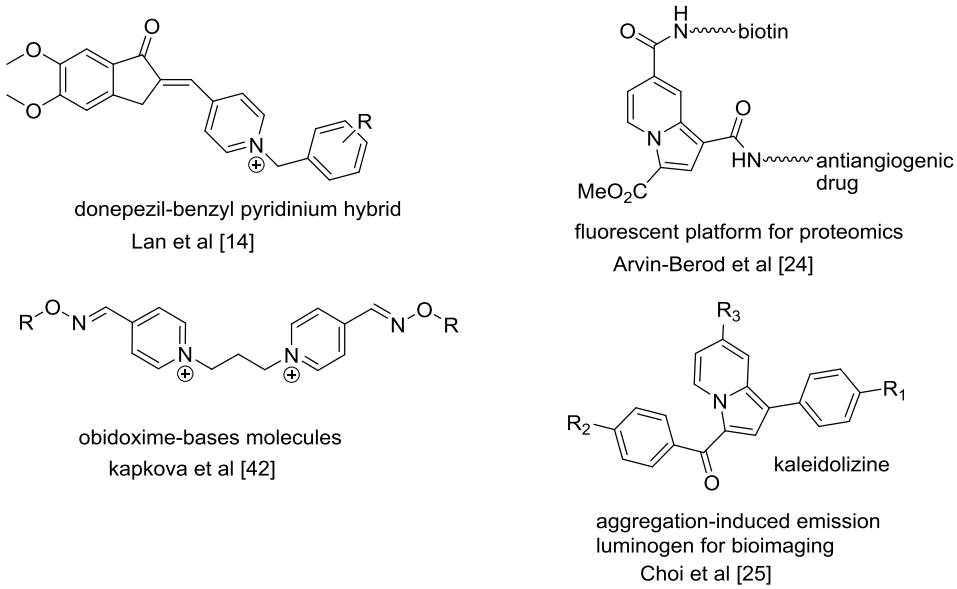

Figure 1. Examples of pyridinium salts and indolizine derivatives of biological interest.

Interestingly in the field of AD, several pyridinium salts have been designed to interfere with ChE activity as mentioned above [9, 10, 14-16, 31-35] and it is worth citing methoxime and obidoxime that are potent agents against nerve toxin action [36]. Both pyridiniums and indolizines compounds also showed significant antioxidant properties [37, 38] or interference with amyloid aggregation [31, 39, 40]. Starting from these considerations it was tempting to evaluate the indolizines and pyridinium derivatives that we are developing in our groups as MTDL's against AD. Three series of derivatives were envisioned as possible candidates: symmetrical bis-pyridinium salts or bis-indolizines, and *N*-alkylpyridinium-indolizine hybrids. However, bis-pyridinium salts are already known structures in this field [15, 41-43], and the low solubility of bis-indolizines in water appeared as a severe limitation to their biological evaluation. Nevertheless, preliminary investigations to this work confirmed the

potential as antioxidant and acetylcholinesterase inhibitors of both symmetrical bis-pyridiniums and bis-indolizines (unpublished data, see SI). To make the most of each heterocycle's properties, we decided to focus on hybrid molecules containing both an indolizine ring and a pyridinium moiety bearing various *N*-substituents.

A first series of *N*-alkylpyridinium-indolizines (Figure 2A, **Ind-PyC0** series, compounds **1-4**) was synthesized previously to this work [44, 45]. We describe here the synthesis of two other series that differ by the length of the aliphatic linker (2 or 3 methylenes for compounds **5-10** and **11-16** respectively), and by the nature of their substituents (Figure 2A). This small library was evaluated against several current AD's targets, i.e. AChE and BChE inhibition, antioxidant activity, and amyloid fibril formation inhibition. The results were compared to those of the corresponding bis-pyridinium salts **17-20** (Figure 2B). Ellman and DPPH assays were used to respectively assess ChE inhibition and antioxidant ability. In an effort to understand the factors involved in cholinesterase inhibition, docking calculations were performed with the most relevant hybrid molecules, and the influence of the structures on the binding modes will be discussed. Finally, the interference of the molecules on amyloid fibrillation was investigated using short peptide models from tau protein [46-49].

A) Hybrids

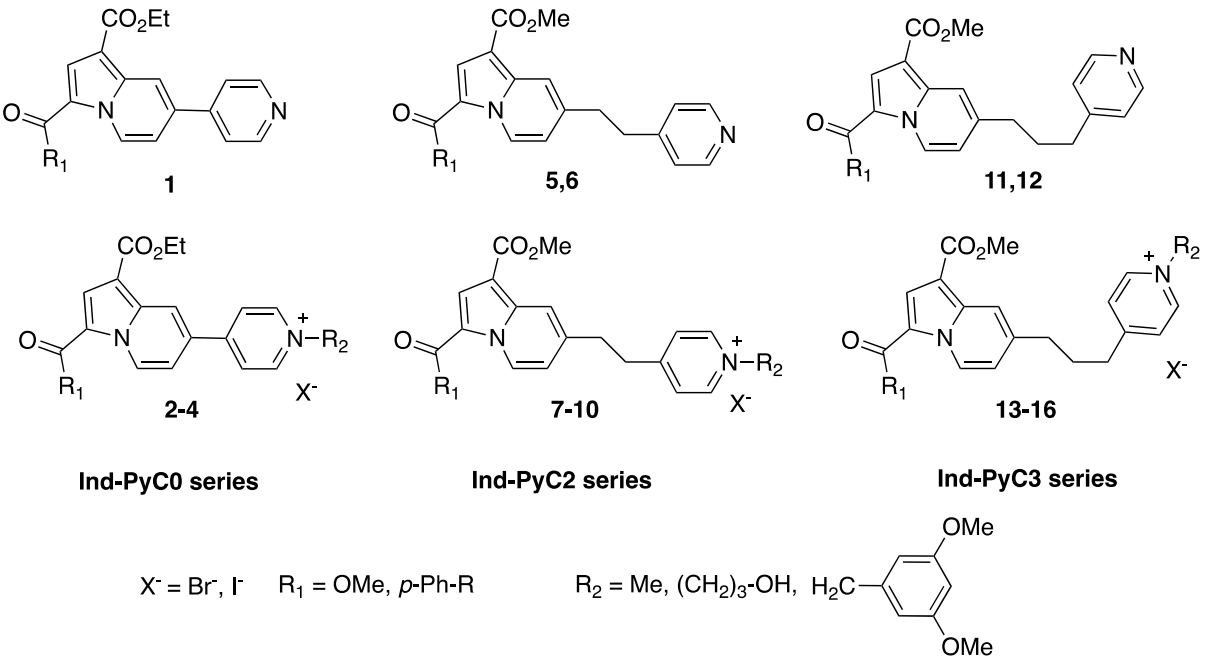

B) Bis-pyridinium salts

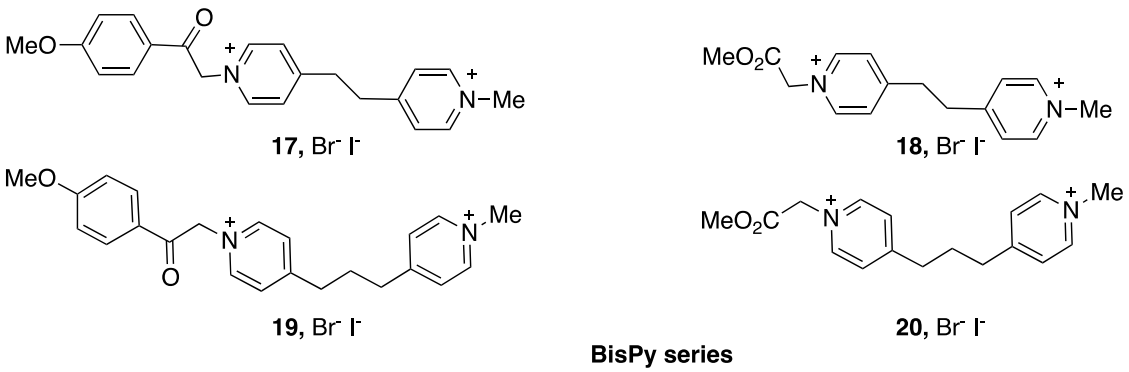

Figure 2. Hybrid molecules and unsymmetrical bis-pyridiniums studied in the present work.

2. Results and discussion

2.1 Syntheses

The first objective was to prepare a series of *N*-alkylpyridinium-indolizine hybrids with structural diversity by both playing with the nature of the starting bis-pyridines and with that of the *N*-alkyl substituents. Two strategies were envisioned to prepare the *N*-alkylpyridinium-indolizine hybrids, both based on the formation of the indolizine ring through 1,3-dipolar cycloaddition of alkynes with the ylides formed in situ from suitably substituted pyridinium salts. The synthetic pathways are depicted in Scheme 1.

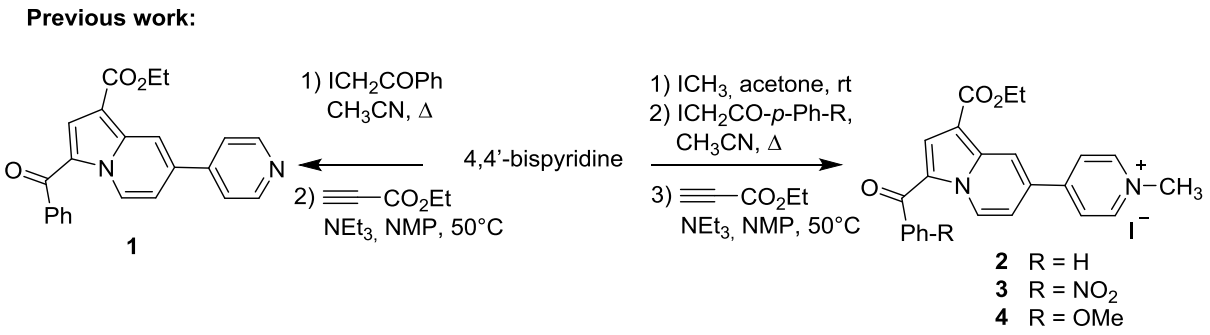

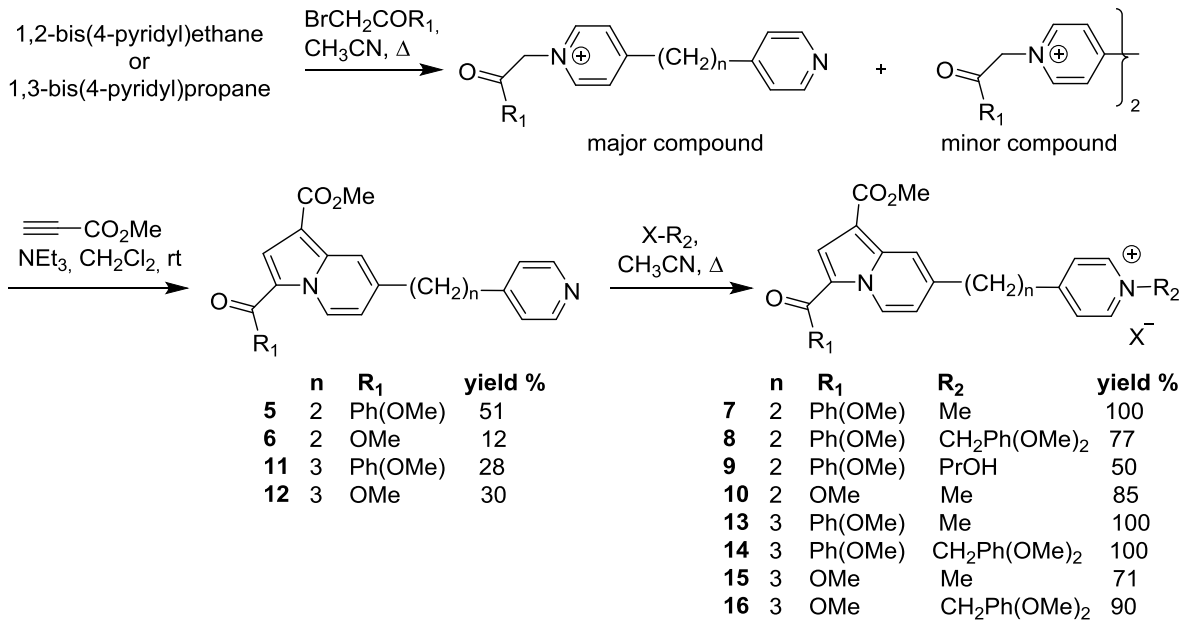

	n	R_1	yield %
5	2	Ph(OMe)	51
6	2	OMe	12
11	3	Ph(OMe)	28
12	3	OMe	30

	n	R_1	R_2	yield %
7	2	Ph(OMe)	Me	100
8	2	Ph(OMe)	$CH_2Ph(OMe)_2$	77
9	2	Ph(OMe)	PrOH	50
10	2	OMe	Me	85
13	3	Ph(OMe)	Me	100
14	3	Ph(OMe)	$CH_2Ph(OMe)_2$	100
15	3	OMe	Me	71
16	3	OMe	$CH_2Ph(OMe)_2$	90

Scheme 1. General route to the *N*-alkylpyridinium-indolizine hybrids of the **Ind-PyC2** and **Ind-PyC3** series. The **Ind-PyC0** compounds have been previously described [44, 45].

As previously described, the **Ind-PyC0** series, **2-4**, were prepared from the non-symmetrical bis-alkylated bipyridinium salts, themselves obtained by controlled mono-methylation of 4,4'-bipyridine followed by a second alkylation with iodoacetophenones [44, 45]. The cyclization

step, with ethyl propiolate, regioselectively occurred on the ylide forming side of the molecules (CH_2COR).
For the **Ind-PyC2** and **Ind-PyC3** series**,** with respectively 2 or 3 carbons between the two rings, the molecules mostly differ by the nature of the pyridinium *N*-alkyl group. It then appeared more time saving to first build the indolizine core, and ultimately quaternize the resulting pyridine-indolizine using various alkylating agents (Scheme 1). In most cases, the first alkylation step was performed at 70-80°C in CH_3CN in the presence of 0.9 to 1 equivalent of the alkylating agent (2-bromo-*p*-methoxyacetophenone or methyl 2-bromoacetate), to give the desired monoalkylated product as major compound (30-85% not optimized yields). In some cases, the mixture of mono- and bis-alkylated compounds thus obtained was directly engaged in the next step. To form the indolizine ring, the reaction with methyl propiolate was achieved at room temperature in CH_2Cl_2 using triethylamine as a base to generate the reactive ylide. The resulting pyridine-indolizines **5**,**6**,**11**,**12** were isolated in 12-51% yields (two steps). The final alkylation step, with various alkylating agents, was done in CH_3CN to give the pyridinium-indolizine salts **7-10**,**13-16** in medium to excellent yields (50-100%).
Four bis-pyridinium salts (**17-20**) were also prepared by controlled mono *N*-alkylation with methyl iodide, followed by the reaction with bromoacetophenone (the structures are depicted in Figure 2).

2.2 ADMET molecular descriptors

Considering the size and the positive charge carried by the hybrids, it appeared important to check their ADMET descriptors. For a long time, uncharged small lipophilic molecules were the only candidates for central nervous system (CNS) targeting, however the discovery of specific Organic Cation Transporters (OCT), enabling charged molecules to pass through the blood brain barrier (BBB) to enter into the brain, changed this paradigm [50, 51]. Actually, most CNS active drugs bear basic amines and are therefore positively charged at pH = 7.4 [52].
To help efficient designing of new molecules as CNS candidates, ADMET rules were adapted and a series of key parameters were selected [52]: 1) Lipophilicity with the calculated partition coefficient LogP, ideally found between 0.4 and 5.1; 2) Distribution at pH = 7.4 with LogD ranging between 0.4 and 3.8; 3) Molecular weight, average = 305; 4) Number of H-bond donors ≤ 2; and 5) Polarity with polar surface area (PSA) ranging between 16 and 86 $Å^2$. This last criterium has been pointed out by other authors as being the most important factor, with PSA<90 [53], along with MW < 450 and LogD ranging between 0 and 3.
We calculated a set of ADMET descriptors. The data are collected in Table S1. For comparison, we also calculated the data for the symmetrical bis-pyridinium salts and bis-indolizines (**1'a-c**/**2'a-c** and **3'a-c**/**4'a-c** respectively, Table S4). It is worth noting the discrepancy that may be found using different calculation softwares, however our purpose was mainly the comparison of closely related structures. All calculations were made using Marvin software.

The pyridine-indolizines (**1**, **5, 6, 11** and **12**) are not or only partly protonated at pH 7.4 (calculated pKa at 4.6 for **1** and 5.6 for the other compounds), leading to a large increase in lipophilicity reflected by higher LogP values. Alkylation of the pyridine ring gives mono-cationic molecules in a large pH range, thus conferring to the molecules ADMET values compatible with CNS potential drugs [54].

In the **Ind-PyC0 series**, the major difference was found with **3**, in which the presence of a nitro group significantly increases the PSA value to 94.8 $Å^2$, i.e. the highest value in this hybrid library, compared to 60.9 $Å^2$ for the methoxy substituted analog **4**.
In the **Ind-PyC2 series** (compounds **7-9**), the nature of the *N*-pyridine substituent (methyl, 3,5-dimethoxybenzyl, 3-hydroxypropyl) influences the PSA values in some extent (from 60.9 to 81.1). Replacing methyl by the bulky 3,5-dimethoxybenzyl group increases LogP value, the more hydrophilic 3-hydroxypropyl group having the opposite effect.
In the C2 and C3 series, exchanging the more hydrophobic *p*-methoxybenzoyl group on indolizine ring by the methyloxycarbonyl group has no effect on PSA, but notably decreases LogP values (from 0.65 for **13** to -0.64 for **15**, or from 2.06 for **14** to 0.77 for **16**). Increasing the length of the linker, from 0 to 3 methylenes, has no effect on PSA, but leads to an increase in lipophilicity (LogP ranging from -0.32 for **4** to 0.65 for **13**).

The BBB penetration ability was estimated using Swiss ADME web service. The results predicted that the molecules showing high PSA and/or LogP (**8**, **9**, **14**, **16**), i.e. containing large lipophilic substituents, are not favorable for BBB crossing. However, the involvement of an active penetration mechanism cannot be ruled out.

2.3. Biological evaluation

2.3.1 Spectroscopic properties

The commonly used methods to evaluate cholinesterase inhibition and antioxidant activity are Ellman's and DPPH assays, respectively. They are both colorimetric spectroscopic assays. The Ellman's method [55] needs 5,5'-dithio-bis-2-nitrobenzoic acid (DTNB) and acetylthiocholine as alternative substrate of the enzyme. The AChE activity, in presence or absence of the tested compounds, is monitored by the formation of the yellow 5-thio-2-nitrobenzoate that absorbs at 405 nm. For the evaluation of antioxidant ability, the assay is based on the reduction of a purple colored DPPH (2,2-diphenyl-1-picrylhydrazyl) that strongly absorbs at 517 nm [56]. DPPH is a free radical that can react with a hydrogen donating antioxidant molecule. The antioxidant effect is then evaluated by following the decrease of the 517 nm absorption. Thus, if the molecules to be tested absorb strongly around either 400 or 500 nm, results of assays may be biased. Absorption of the tested molecules is also of importance when studying their effect onto amyloid fibril formation by the fluorescence Thioflavin (ThT) assay [57, 58]. ThT assay is based on the fluorescence of the ThT dye in presence of the characteristic β-sheet motif of amyloid fibril in formation. The use of blank controls makes it possible to assess the intrinsic fluorescence of compounds which could lead to erroneous interpretations. However, ThT assay may also be biased by the inner filter effect of compounds with strong absorption at 440 nm or/and 480 nm, corresponding to excitation and emission wavelengths of the bound ThT [59, 60].
In light of this, we first recorded the UV/Vis absorption of all the molecules to check if their own spectroscopic properties would interfere with the assays (Figure S1). Except for the uncharged hybrid **1**, the **Ind-PyC0** molecules strongly absorb around 415 nm due to their extended conjugation, as observed previously [44], making impossible their evaluation with both Ellman's and ThT assays. For all other compounds, maximum UV/Vis absorptions around 325 or 375 nm are suitable for the three assays.

2.3.2 Antioxidant properties

Oxidative stress is involved in age related neurodegenerative diseases and in particular in AD. Thus, antioxidants may have positive benefits in reducing or delaying neuronal death. The antioxidant properties of the molecules were evaluated by DPPH radical scavenging. The 1,1-diphenyl-2-picrylhydrazyl or DPPH is a stable free radical characterized by a deep violet color, with an absorption band in ethanol solution at 517 nm. In the presence of a molecule that can donate a hydrogen atom, the formation of reduced DPPH is accompanied with the loss of this violet color. Rutin was used as reference. The DPPH inhibition % which relates to antioxidant activity was calculated at 48 µg/ml drug concentrations (i.e. the concentration for which rutin gives 83.3±0.1 inhibition% in our assay), 188 and 750 µg/ml drug concentrations (Figure 3) [61]. All the molecules have been tested, however as indicated in Table S2, some molecules (compounds **1** and **3** from the **Ind-PyC0** series and the uncharged compounds **5** and **11**) displayed an unacceptable standard deviation due to precipitation issue and are not therefore indicated in the Figure 3.

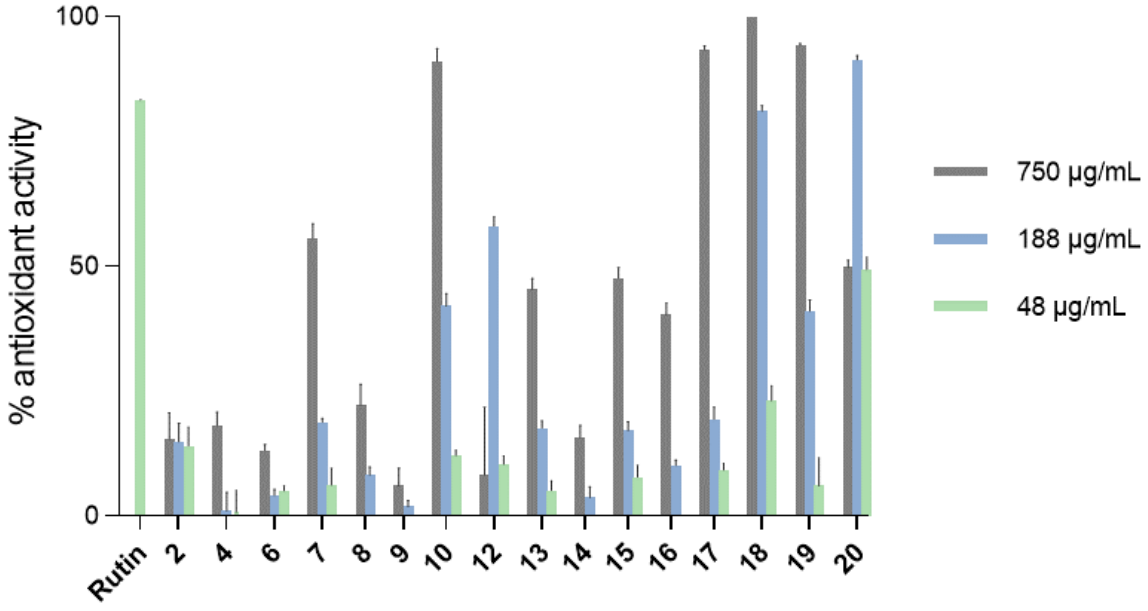

Figure 3. Antioxidant activity (%) is measured using DPPH assay at 48 µg/ml (green), 188 µg/ml (blue) or 750 µg/ml (grey) drug concentrations, rutin was used as reference. All assays were performed in triplicate and each bar value corresponds to the mean ± SD. Both the values with unacceptable SD and closed to zero are not represented (see Table S2).

.

Most of the molecules showed no or low activity when dosed at 48 µg/ml, except with the bis-pyridinium salt **20**, significantly active at that concentration (around 50% inhibition). However, rising the drug concentration up to 750 µg/ml led to a significant increase in efficiency for most compounds, and in particular the bis-pyridinium **17-19** showed up to >90% inhibition. Among the hybrids, the neutral compound **12** seemed promising with near 60% inhibition at 188 µg/ml, but solubility issues prevented correct measurements at higher concentration. Compound **10** showed the highest antioxidant properties (about 90% inhibition) at 750 µg/ml. Note that we observed similar trends with the previously described symmetrical analogs: bis-pyridinium salts showed better activity compared to bis-indolizines (compare **1'** and **2'** series vs **3'** and **4'** series, Table S4).

2.3.3 Cholinesterase inhibition

2.3.3.1 IC_{50} determination

The cholinesterase activity was evaluated using the Ellman's spectrophotometric method [55] against electric eel AChE (eeAChE) and equine butyrylcholinesterase (eqBChE), and selected compounds have been further tested against the human enzymes (hAChE and hBChE).

Our goal being to select molecules that would significantly inhibit cholinesterases, a rapid screening of all series was first performed at 4 µM against eeAChE and eqBChE (see Figure S2 to S5). Only the molecules that inhibited at least 50% of the ChE activity at this micromolar concentration were then evaluated in a larger concentration range to precisely calculate IC_{50} values. The data are collected in Table 1 (see also Table S3 for the IC_{50} curves).

Table 1. Cholinesterase inhibition. [a,b]

Ind-PyC2		**6**	**7**	**8**	**10**		**9**
ee AChE		Inact.[c]	4.4±0.5	Inact.[c]	5.4±0.1		2.0±0.4
eqBChE		Inact.[c]	17.5±8.2	Inact.[c]	55.4±2.3		8.8±3.5
hAChE		nd	6.6±1.1	nd	37.1±4.1		8.0±0.9
hBChE		nd	nd	nd	nd		nd
Ind-PyC3	**11**	**12**	**13**	**14**	**15**	**16**	**Donepezil[e]**
eeAChE	Inact.[c]	Inact.[c]	2.6±0.6	> 10µM [d]	7.9±0.6	2.7±0.6	0.052±0.007
eqBChE	Inact.[c]	Inact.[c]	7.5±3.4	4.8±1.3	72.1±15.9	7.3±1.2	6.0±1.7
hAChE	nd	nd	3.3±0.7	nd	4.0±0.9	9.4±2.5	0.029±0.005
hBChE	nd	nd	38.9±14.0	nd	> 100 µM	nd	9.2±5.6

[a] IC_{50} values in µM are expressed as mean±standard error of three independent experiments performed in triplicates; [b] For easier comparison of C2 versus C3 series, the molecules containing the same substituents are represented in the same column; [c] The molecules indicated as inactive did not show significant activities during a first rapid screening at 4 µM (Figures S3 to S6); [d] Formation of aggregates at higher concentrations in presence of eeAChE; [e] Donepezil is used as control (see Table S3 and Figure S7 for IC_{50} curves).

The already mentioned strong UV-Vis absorbance of the **Ind-PyC0** molecules, along with their lower solubility in water, prevented their study in a large range of concentrations, and

the promising effects obtained in the 4 µM screenings, especially for **2** and **3** against eeAChE, could not be confirmed (see Figures S3). The bis-pyridinium salts **17-20** did not show any significant inhibition properties against the two enzymes at 4 µM (Figure S5). Similarly, the uncharged pyridine-indolizines (**6**, **11** and **12)** are inactive against both enzymes (Figure S4). As expected, most of the corresponding symmetrical cationic pyridine-indolizine hybrids were active at 4 µM. Unlike what was previously observed with most of bis-indolizines (see Table S4) that easily form aggregates in aqueous solutions, the generally better solubility of the pyridinium-indolizine hybrids allowed their evaluation in a larger concentration range.
Thus, the cationic hybrids displayed micromolar IC_{50}, with a slight selectivity for eeAChE vs eqBChE (Table 1), except **10** and its analog **15,** which showed the highest selectivity (being 10 times more active against eeAChE compare to eqBChE) [62].
The **Ind-PyC3** molecules containing the 3-*p*-methoxybenzoyl group appeared more active against the two enzymes than their **Ind-PyC2** analogs (compare **13** and **14** with **7** and **8**, respectively). This effect may be related to the better flexibility of the propyl linker compared to the shorter ethyl one. Concerning the eeAChE inhibition, the pyridinium-indolizine hybrid **8** was the only inactive hybrid. This hybrid bears the lipophilic bulky *N*-dimethoxybenzyl group along with the 3-*p*-methoxybenzoyl substituent. Its **Ind-PyC3** analog **14** displayed more interesting activities against both enzymes, however a closer look to the curves and Prism calculations (Table S3) showed that its limited solubility in presence of eeAChE at concentrations higher than 10 µM leads to a decreased R-squared value compared to the other tested molecules. Compound **16**, analog of **14** in which the 3-*p*-methoxybenzoyl was replaced by the smaller size methyloxycarbonyl group, exhibited a good activity against both eeAChE (IC_{50} = 2.7 µM) and eqBChE (IC_{50} = 7.3 µM) without any apparent solubility limitation.

Due to the high costs of the human cholinesterases, only a few active molecules were then selected for further evaluation (Table 1, and Figure S7 for IC_{50} curves). For most tested compounds, IC_{50} against hAChE remained in the same micromolar range, except for **10** that lost activity with IC_{50} > 30 µM for hAChE. Two molecules, **13** and **15**, that only differed by the nature of the substituent at position 3 of the indolizine ring, were also tested against hBChE. The efficiency of **13**, that previously showed a significant micromolar IC_{50} value against eqBChE, strongly decreased (IC_{50} / 5) against hBChE. Compound **15** was not active (IC_{50} > 100 µM) confirming its previously observed selectivity for AChE vs BChE.

The indolizine derived molecules reported in this study contain at least one carboxylic ester function. Considering the hydrolase activity of the tested enzymes, we wondered if these esters could be substrates of these enzymes [63]. To answer this question, the behavior of **15**, containing two methyl esters groups at positions 1 and 3 of the indolizine ring, was studied in presence of either hAChE or hBChE and of their respective substrates (acetyl- or butyrylthiocholines). The reactions were monitored by HPLC using a diode array detector, and after one day of reaction the organic compounds were extracted from the pH8 buffer by dichloromethane. After evaporation of the organic phases, the residues were dissolved in deuterated chloroform to perform ^{1}H NMR analysis. Neither retention time nor absorbance values appeared modified on the HPLC chromatograms. The NMR data corresponded to a mixture of the starting diester **15** and of thiocholine (Figure S2). However, the integration of the peaks at 3.95 ppm corresponding to the two OCH_3 appeared slightly smaller than expected for the diester, which may indicate the presence of a small amount of partly hydrolyzed **15**. The close proximity of the two OCH_3 peaks did not allow the identification of the ester that was preferentially hydrolyzed. The dichloromethane extraction from the pH8 buffer used to perform the enzymatic reaction constituted a limitation to this study as the hydrolysis of **15**

would give either a zwitterion (mono-hydrolysis) or a negatively charged diacid (bis-hydrolysis), that would be difficult to extract from the basic medium.
However, this study clearly showed that after one day of reaction, a significant amount of diester **15** was still present in solution, but a partial hydrolysis could not be ruled out from the NMR analysis.

2.3.3.2 Docking calculations

Docking calculations were then performed to compare the possible binding modes of compounds **13** and **15** within the active sites of the two human ChE. Indeed, whilst both are active as inhibitors of AChE (eel or human), they showed a different behavior on BChE (equine or human).
It is challenging to design a good inhibitor that would be active on both hAChE and hBChE, as these two enzymes differ considerably in size (hAChE binding site is much smaller than hBChE) and in composition (residues W286, V294, Y124, Y337, F297 in hAChE are respectively A277, P285, Q119, A328 and V288 in hBChE).
Compounds **13** and **15** showed Glide docking scores of respectively -11.3 and -9.3 kcal/mol in hAChE, and -9.1 kcal/mol and -8.5 kcal/mol in hBChE. These theoretical affinity patterns are consistent with experimental IC_{50}, **13** being more active than **15** on both enzymes (Table 1).

In the hAChE active site (Figure 4), the best pose of **13** had a pyridinium moiety oriented towards the bottom of the catalytic site, in the immediate vicinity of E202 and of the catalytic serine S203 (Figure 4b).

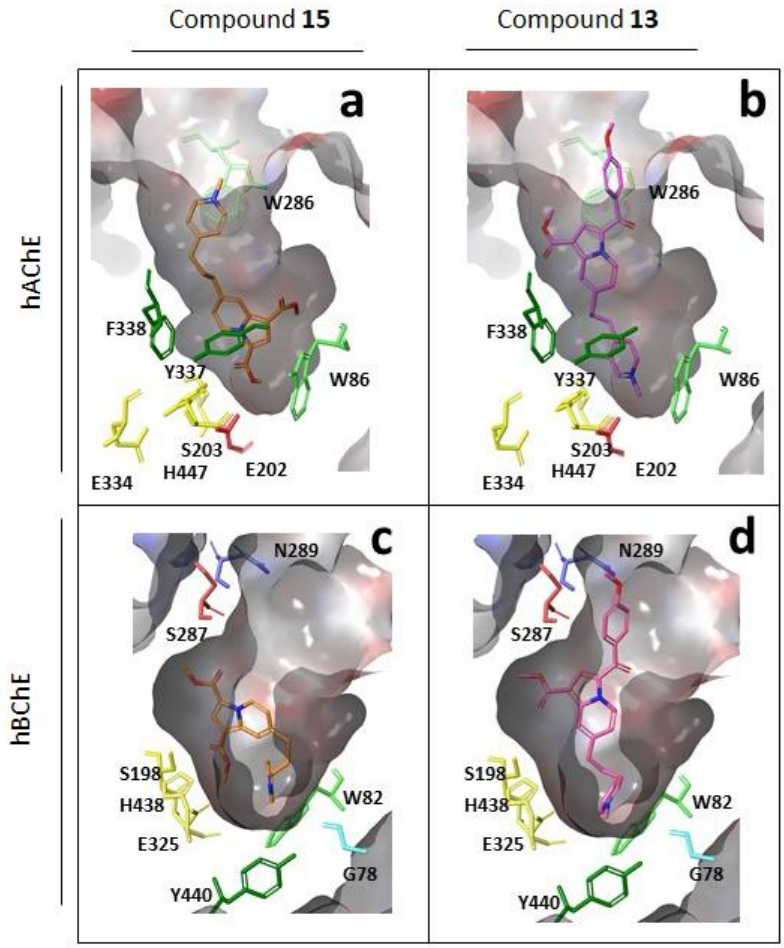

Figure 4. In a and b are illustrated the binding site of hAChE with respectively docked **15** and **13**. In c and d are respectively drawn the best docked poses of **15** and **13** in the hBChE binding pocket. The catalytic residues are in yellow.

This binding mode was fully conserved among the 20 best poses of **13**, probably driven by the stabilizing interaction with E202 negative charge. Thus, **13** is not in a suitable position for hydrolysis by the hAChE enzyme. Compound **15** with a small methyl ester group was oriented inversely compared to **13**: the pyridinium group towards the entrance of the cavity, and the methyl ester group at position 3 facing the catalytic triad at the bottom, allowing a possible hydrolysis (Figure 4a). The indolizine moiety is surrounded by residues W86, Y337, F338 and the pyridinium moiety is in π-stacking interactions with W286. Due to its smaller size, **15** showed more heterogeneity among the binding poses. One of them, with the pyridinium moiety oriented towards the catalytic pocket and a salt bridge with E202 showed a close docking score of -8.8 kcal/mol. These data are consistent with the similar activity observed for both **13** and **15** in hAChE.

In the hBChE binding site, **13** preferentially found its position with its pyridinium moiety inserted at the bottom of the site, close to the catalytic H438; the charge is stabilized by the hydroxyles of Y332 and Y440 tyrosines, and by three carbonyl groups of residues A328 G78 H438 (Figure 4d). Residue W82 provides a favorable π-stacking interaction to the pyridinium group. The methyl ester moiety is located at less than 5 Å to the catalytic S198, and we hypothesize that this compound may adopt a closely-related binding mode to the natural substrate butyrylcholine. This binding mode was very conserved among the twenty best poses

of **13**. The best position of **15** showed its pyridinium moiety oriented towards the bottom of the cavity, where it is stabilized by the carbonyl oxygen of A328 (Figure 4c). The methyl ester at position 1 is in a perfect position for hydrolysis by S198.
Compounds **13** and **15** showed a conserved orientation of their pyridinium moieties within the hBChE pocket, but a reverse positioning of this group in hAChE: **13** has its pyridinium group towards the CAS site, whereas **15** has its pyridinium group towards the entrance of the cavity. Residue W286, which is an alanine in hAChE, is in pi-stacking interaction with the benzoyl substituent of **13** and the pyridinium of **15**.
Concerning the diester **15**, it is worth noting that with both enzymes, one methyl ester is in good position for hydrolysis, in agreement with the NMR study analysis.

2.3.4 Amyloid fibrillation inhibition

To monitor the effect of molecules on the amyloid fibrillation process, thioflavin-based fluorescence assay is generally used as it is highly sensitive to the β-sheet motifs of fibers. Upon binding to fibers, ThT displays a red shifted emission allowing the selective detection of β-sheet rich structures such as fibers. We used here two models of amyloid peptides, both derived from the tau protein sequence (Figure 5).

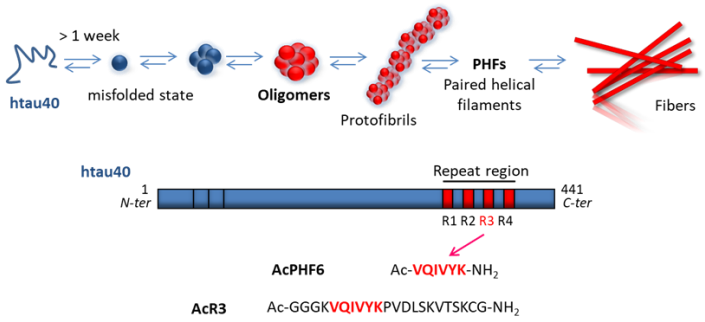

Figure 5. Tau fibrillation process (in red β-sheet containing species), and sequences of the two tau models used in this study.
The AcPHF6 model is a short 6 amino-acid length peptide corresponding to the core of tau fibrils [49]. Its fibrillation is much faster than those of tau protein or amyloid peptides that can take days, and it is well adapted for a first screening of a set of molecules by ThT fluorescence assays. We already set up in previous works such screening in 96-well microplates to study a series of aurones [46]. In addition, we used a longer peptide derived from the R3 repeat tau region, AcR3, which has been developed in our group (unpublished data). The studies were performed in phosphate buffer, and the ThT fluorescence signal was recorded in absence and in presence of the **Ind-PyCx** and **BisPy** molecules at a 100 µM concentration (corresponding to a 1/1 ratio with the amyloid peptide). With AcR3 model, heparin was added as fibrillation inducer, and 10 µM of heparin corresponding to 0.1/1 ratio with this amyloid peptide was used. Results reported in figure 6 are expressed as the percentage of ThT fluorescence inhibition. Blank wells were used to heed any intrinsic fluorescence emission of the hybrids. No additional fluorescence to that of free ThT was detected in these controls.

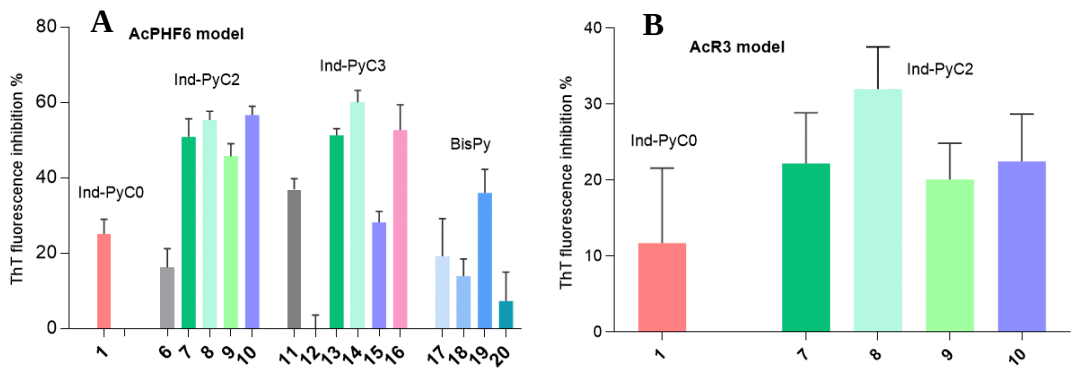

Figure 6. ThT assays on AcPHF6 (A) and AcR3 (B) models of amyloid fibers (λ_{exc} = 440 nm, λ_{em} = 480nm). The results are expressed as the inhibition % of ThT fluorescence using a ratio compound/model of 1/1 (100 µM concentration). The errors represent the SEM of three independent experiments performed in triplicates.

As shown in figure 6A, most of the **Ind-PyC2** and **Ind-PyC3** hybrids displayed some activities on AcPHF6 model. The **BisPy** references **17-20** or the uncharged compound **6** and **12** were significantly less efficient. The length of the Cx linker did not seem to play an important role as similar activities were observed with both **Ind-PyC2** and **Ind-PyC3** series. At first glance, the nature of the substituents carried by each hybrid did not seem to be important either.
To go further, we decided to evaluate on the longer peptide model AcR3 the four most active **Ind-PyC2** compounds (**7-10**) as well as the **Ind-PyC0 1**. The inhibition efficiency was then divided at least by a factor two (compare Figure 6A and 6B).

It is noteworthy that inhibition of fluorescence in ThT assays does not necessarily mean inhibition of amyloid fiber formation. Indeed, displacement of the bound ThT by the tested compounds may also occur. Consequently, we prepared a solution of AcR3 fibers in the presence of ThT and recorded the bound ThT signal before and right after adding the compounds of the **Ind-PyC2** series (Figure 7A, dotted lines). No decrease of ThT signal at 480 nm was observed suggesting that compounds are not able to displace the bound dye. The same observation was made with compound **1**. To ensure that the recorded signal was still from bound ThT, we checked that the compounds fluorescence did not significantly light up in presence of preformed fibers at the working wavelengths (Figure 7A, solid lines). However, the slight increase and red shift of the fluorescence signal observed in Figure 7A (dotted lines) upon addition of the charged molecules **7-9** is probably due to this additional fluorescence, even weak, and suggests that **7-9** interact closely with fibers. This is confirmed by their huge fluorescence emission in presence of fibers when excited at their absorbance maximum while they are no fluorescent alone (Figure 7B). Compound **10**, which bears two ester groups on its indolizine part (**7** being its 3-*p*-methoxybenzoyl analog), is the exception to the rule. Interestingly, analogs **14** and **16** from the **Ind-PyC3** series exhibited the same behavior (Figure S8): **16** with two ester groups did not show a significative emission in presence of AcR3 fibers in contrast to **14**, suggesting the importance of the benzoyl substituent onto the indolizine part for a greater interaction with fibers.

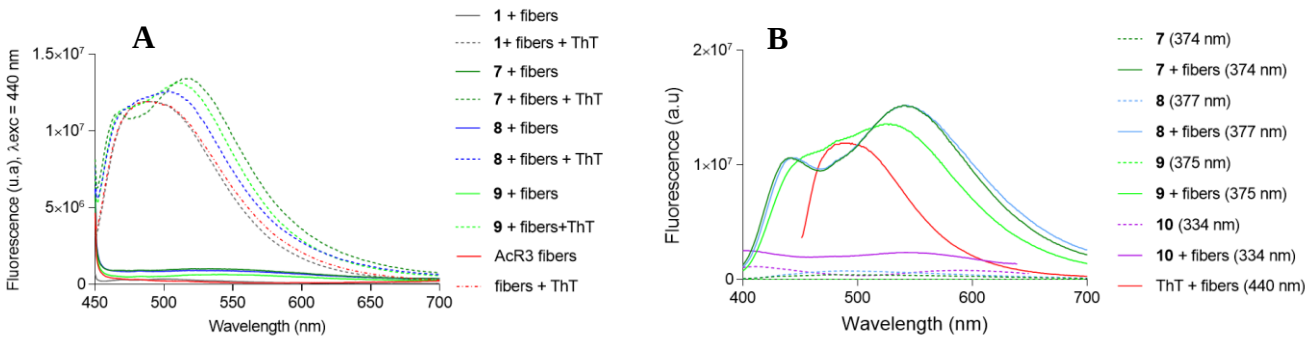

Figure 7. (A) ThT displacement assay. The excitation wavelength is 440 nm. The ratio compound/ThT is 10/1 (100/10 µM) and the AcR3 fibers have been prepared from 100 µM of peptide in absence (solid lines) or in presence of ThT (dotted lines). (B) Fluorescence emission of **Ind-PyC2** compounds (100 µM) alone (dotted lines) or in presence of 100 µM of pre-formed fibrils (solid lines). The excitation wavelength corresponds to their absorbance maximum (value in parentheses); ThT in presence of fibers is used for comparison.

Note that in the **Ind-PyC0** series only the uncharged compound **1** was evaluated by ThT assay (Figure 6). Indeed, as explained before, the strong absorption of compounds **2-3** around 415 nm, and in addition the strong fluorescence of **2** and **4** in the wavelength range of bound ThT fluorescence emission did not permit their evaluation [44] (Figures S1 and S9).
Thus, to study the interaction of the **Ind-PyC0** molecules, we used the circular dichroism spectroscopy (CD) that provides structural information on amyloid peptides during the aggregation process. The CD spectra of AcR3 peptide were registered in phosphate buffer in presence of heparin as fibrillation inducer. They displayed the typical profile of a peptide with a high fraction of β-sheet structures, characterized by a broad negative shoulder around 218 nm (Figure 8, red color) in less than 24h at 37°C. No significative difference was noticed when compounds **1-4** were added to the fibrillation mixture (Figure 8A) attesting that compounds of **Ind-PyC0** series did not impede the formation of β-sheet structures (note that the positive shoulder of β-sheet profile under 200 nm cannot be observed due to the strong absorption of DMSO used for the dilution of compounds). These results tend to show that **1-4** do not inhibit fibers formation, or at least the formation of β-sheet-rich structures.

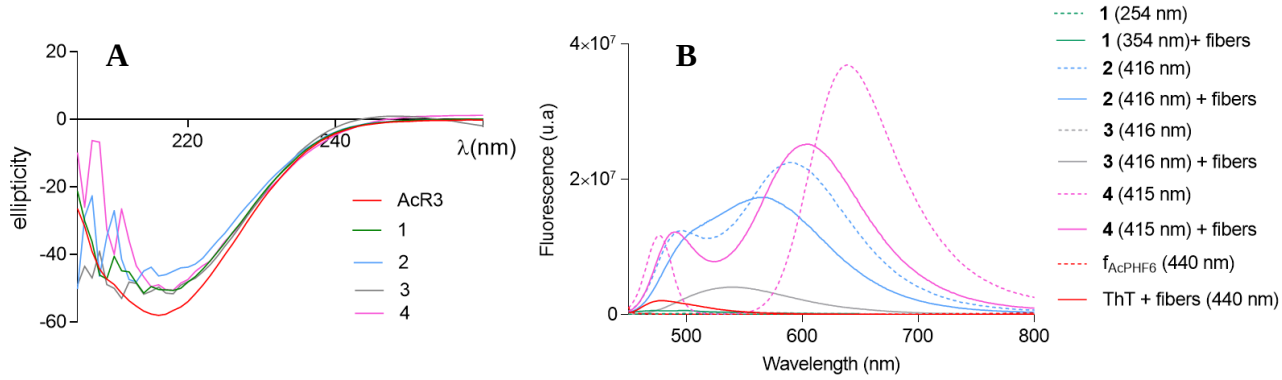

Figure 8. (A) CD spectra obtained after a 24h incubation at 37°C of AcR3 at 100 µM, alone (red) or in presence of 100 µM of **Ind-PyC0** series **1 to 4**. (green, blue, grey and pink). 10 µM heparin is used as fibrillation inducer. (B) Fluorescence emission of **Ind-PyC0** series

(100 µM) alone (dotted lines) and in presence of 100 µM of pre-formed AcPHF6 fibrils (solid lines). The excitation wavelength corresponds to their absorbance maximum (value in parentheses); 10 µM ThT in presence of fibers is used for comparison (red solid line).

Then, we recorded their fluorescence in presence of preformed fibers as described above for the **Ind-PyC2** series. With the most fluorescent compounds **2** and **4,** we observed an increase of their fluorescence maximum with a slight red shift in presence of AcPHF6 fibers (Figure 8B). Such modification in the emission spectra may be explain by a close interaction with fibers.
More interestingly, among the non-fluorescent compounds **1** and **3**, only **3** showed a fluorescence light-up in presence of AcPHF6 fibers (Figure 9A). In addition, the fluorescence intensity is much higher compared than that of the bound ThT dye at the same concentration.

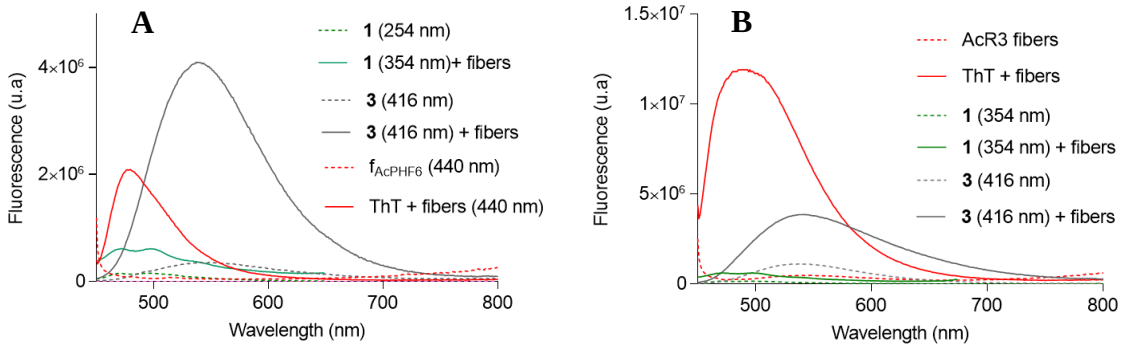

Figure 9. Fluorescence emission of compounds **1** and **3** (100 µM) alone (dotted lines) and in presence (solid lines) of (A) 100 µM of pre-formed AcPHF6 fibrils or (B) 100 µM of pre-formed AcR3 fibrils (B). The excitation wavelength corresponds to their absorbance maximum (value in parentheses); 10 µM ThT in presence of fibers is used for comparison.

The same response was observed, to a lesser extent, in the case of AcR3 fibers (Figure 9B and Figure S10). Further study would be needed, but **3** could be of interest as reporter dye of fibrillation. The fluorescence of **3** being red-shifted in comparison to ThT (550 nm vs 480 nm), it would allow screening of a wider range of potential inhibitors

3. Conclusion

In the course of this study, we have synthesized and evaluated a series of 20 molecules, bis-pyridinium salts and pyridinium-indolizine hybrids. The molecules were tested against AD hallmarks, i.e. antioxidant properties, inhibition of AChE and BChE, and interference with amyloid fibrillation using tau peptide models. The hybrids are constituted of an indolizine core linked to a pyridinium pendant, and they differ by the length of the linker, with 0, 2 or 3 methylene units (**Ind-PyC0**, **Ind-PyC2** and **Ind-PyC3**, respectively). The substituents at position 3 of the indolizine and on the heterocyclic pyridine nitrogen were also varied. No hybrid showed significant activity on the three targets simultaneously, i.e. antioxidant activity (DPPH inhibition %> 50 at 48 µg/mL), hChE inhibition (IC_{50} < 10 µM) and inhibition of amyloid fiber formation. The **Ind-PyC2** and **Ind-PyC3** series were weak anti-oxidants, and moderate inhibitors of amyloid fibers formation. However, most of the positively charged molecules from these two series are active on both eeAchE and hChE at micromolar range. A

few molecules also inhibited eqBChE but unfortunately not the human enzyme hBChE. The **Ind-PyC0** series showed a significantly different behavior from the other two series. Both solubility limitation (the molecules are prone to aggregate in water solution) and spectral properties did not allow their study neither as cholinesterase inhibitors nor as fibers inhibitors. Nevertheless, in the amyloid fiber context, fluorescence and CD experiments revealed that if these molecules don't interfere in the fibrillation process, the positively charged **2-4**, and in particular the nitro derived **3**, may be new fluorescent reporter dyes of amyloid fiber formation.

4. Material and methods

4.1 Synthesis

NMR spectra were recorded at room temperature in 5 mm tubes on a Bruker AC 400 MHz spectrometer (NMR facility, PCN-ICMG, Grenoble). Chemical shifts (δ) are reported in parts per million (ppm) from low to high field and referenced to residual non-deuterated solvent relative to Me_4Si. Standard abbreviations for multiplicity were used as follows: s = singlet; d = doublet; t = triplet; m = multiplet. High resolution mass sectrometry (HRMS) was carried out on a Bruker UHR-Q-TOF MaXis-ETD (Time of Flight) mass spectrometer using ElectroSpray Ionisation (ESI) in Institut de Chimie Organique et Analytique (CBM-ICOA) in Orleans (France).

The *N*-alkylpyridinium-indolizines **1-4** of the **Ind-PyC0 series** [44, 45] and the bis-pyridinium salt **17**[64] have already been described.

4.1.1 Ind-PyC2 series

4.1.1.1 Methyl 3-(p-methoxybenzoyl)-7-[2-(4-pyridinyl)ethyl] indolizine-1-carboxylate **(5)**

This compound was prepared in two steps from 1,2-bis(4-pyridyl)ethane:

1) *N*-Alkylation

1,2-Bis(4-pyridyl)ethane (504 mg, 2.7 mmol) was dissolved in CH_3CN (7 mL). 2-Bromo-*p*-methoxyacetophenone (1 eq.) was added and the solution was stirred at 70-80°C for 2 h. The yellow precipitate was filtrated and dried under vacuum to give pure 1-(2-(4-methoxyphenyl-2-oxoethyl)-4-[2-(4-pyridinyl)ethyl]pyridinium bromide in 85% (945 mg).

^{1}H NMR (400MHz, CD_3OD) δ 8.77 (d, 2H, *J*=6.4 Hz), 8.49 (d, 2H, *J*=6.0 Hz), 8.10 (m, 4H), 7.41 (d, 2H, *J*=6.0 Hz), 7.16 (d, 2H, *J*=8.8 Hz), 5.53 (s, 2H), 3.97 (s, 3H), 3.44 (t, 2H, *J*=7.8 Hz), 3.24 (t, 2H, *J*=7.8 Hz); ^{13}C NMR (100 MHz, D_2O) δ 190.8, 165.0, 163.0, 150.5, 148.8, 145.1, 131.2, 128.0, 126.1, 124.7, 114.7, 55.9, 35.5, 34.1; HRMS (ESI) m/z: calcd. for $C_{21}H_{21}N_2O_2$ $[M]^+$ 333.1597, obsd 333.1595 and calcd. for $C_{21}H_{22}N_2O_2$ $[M+H]^{2+}$ 167.0835, obsd 167.0838.

2) Indolizine formation

The pyridinium salt thus obtained (600 mg, 1.45 mmol) and methyl propiolate (2.2 eq.) were dissolved in anhydrous CH_2Cl_2 (10 mL). NEt_3 (1.1 eq.) diluted in 5 mL of anhydrous CH_2Cl_2 was then added dropwise in the reacting mixture. After 5 h stirring at rt, water was added to

the solution. The organic phase was separated and washed 2 more times with water before being dried on $MgSO_4$ and concentrated under reduced pressure. The residue was then purified by flash chromatography on silica gel (CH_2Cl_2/MeOH: 98/2) to obtain indolizine **5** in 61% yield.

^{1}H NMR (400MHz, $CDCl_3$) δ 9.84 (dd, 1H, *J*=7.2, 0.8 Hz), 8.56 (d, 2H, *J*=4.4 Hz), 8.21 (d, 1H, *J*=0.8 Hz), 7.87 (d, 2H, *J*=8.8 Hz), 7.82 (s, 1H), 7.41 (d, 2H, *J*=6.0 Hz), 7.18 (d, 2H, *J*=4.4 Hz), 7.04 (d, 2H, *J*=8.8 Hz), 6.92 (dd, 1H, *J*=7.2, 2.0 Hz), 3.94 (s, 3H), 3.93 (s, 3H), 3.09 (m, 4H); ^{13}C NMR (100 MHz, $CDCl_3$) δ184.4, 164.6, 162.6, 149.9, 149.5, 141.3, 140.0, 132.3, 131.2, 128.9, 128.5, 123.9, 122.5, 117.7, 116.4, 113.7, 104.9, 55.5, 51.2, 36.1, 35.7; HRMS (ESI) m/z: calcd. for $C_{25}H_{23}N_2O_4$ $[M+H]^+$ 415.1652, obsd 415.1655.

4.1.1.2 Methyl 3-(p-methoxybenzoyl)-7-[2-(1-methylpyridinium-4-yl)ethyl]indolizine-1-carboxylate iodide **(7)**

The indolizine **5** (372 mg, 0.9 mmol) was dissolved in CH_3CN (8 mL). Iodomethane (1.5 eq.) was added and the solution was stirred at 50°C for 4 h. After concentration under vacuum, the brown residue was washed with CH_2Cl_2. After drying, the *N*-alkylpyridinium-indolizine **7** was thus isolated as a brown solid with a quantitative yield.

^{1}H NMR (400MHz, $CDCl_3$) δ 9.70 (d, 1H, *J*=7.2 Hz), 9.04 (d, 2H, *J*=6.4 Hz), 8.05 (s, 1H), 7.87 (d, 2H, *J*=6.4 Hz), 7.74 (d, 2H, *J*=8.4 Hz), 7.69 (s, 1H), 6.94 (s, 1H), 6.93 (d, 2H, *J*=8.8, Hz), 4.57 (s, 3H), 3.83 (s, 3H), 3.82 (s, 3H), 3.30 (t, 2H, *J*=7.8 Hz), 3.13 (t, 2H, *J*=7.8 Hz); ^{13}C NMR (100 MHz, $CDCl_3$) δ184.4, 164.6, 162.7, 161.0, 145.1, 139.6, 139.2, 132.1, 131.2, 129.3, 128.5, 128.3, 122.7, 117.9, 116.3, 113.8, 105.1, 55.5, 51.4, 49.1, 36.2, 35.0; HRMS (ESI) m/z: calcd. for $C_{26}H_{25}N_2O_4$ $[M]^+$ 429.1809, obsd 429.1810.

4.1.1.3 Methyl 3-(p-methoxybenzoyl)-7-[2-(1-[(3,5-dimethoxyphenyl)methyl]pyridinium-4-yl)ethyl] indolizine-1-carboxylate bromide **(8)**

The indolizine **5** (125.5 mg, 0.3 mmol) was dissolved in CH_3CN (3 mL). 3,5-Dimethoxybenzyl bromide (1.2 eq.) was added and the solution was stirred at 70-80°C for 3 h. After concentration under vacuum, the brown residue was washed with CH_2Cl_2. After drying, the residue was then purified by flash chromatography on silica gel (CH_2Cl_2/MeOH: 90/10) to obtain the *N*-alkylpyridinium-indolizine **8** as a brown solid in 77% yield.

^{1}H NMR (400MHz, $CDCl_3$) δ 9.73 (d, 1H, *J*=7.2 Hz), 9.30 (d, 2H, *J*=6.0 Hz), 8.07 (s, 1H), 7.80-7.42 (m, 4H), 7.70 (s, 1H), 6.94 (s, 1H), 6.93 (d, 2H, *J*=8.8, Hz), 6.87 (dd, 1H, *J*=7.2, 1.6 Hz), 6.73 (d, 2H, *J*=2.0 Hz), 6.37 (d, 1H, *J*=2.0 Hz), 6.03 (s, 2H), 3.83 (s, 3H), 3.82 (s, 3H), 3.71 (s, 6H), 3.23 (t, 2H, *J*=7.6 Hz), 3.09 (t, 2H, *J*=7.6 Hz); ^{13}C NMR (100 MHz, $CDCl_3$) δ184.5, 164.6, 162.7, 161.7, 161.1, 144.5, 139.7, 139.1, 134.6, 132.2, 131.2, 129.3, 128.4, 128.0, 122.7, 117.8, 116.0, 113.8, 107.5, 105.1, 102.0, 63.9, 55.9, 55.5, 51.3, 36.0, 34.8; HRMS (ESI) m/z: calcd. for $C_{34}H_{33}N_2O_6$ $[M]^+$ 565.2333, obsd 565.2337.

4.1.1.4 Methyl 3-(p-methoxybenzoyl)-7-[2-(1-(3-hydroxypropyl)pyridinium-4-yl)ethyl] indolizine-1-carboxylate bromide **(9)**

The indolizine **5** (231.5 mg, 0.56 mmol) was dissolved in CH_3CN (5 mL). 3-Bromo-1-propanol (3 eq.) was added and the solution was stirred at 70-80°C for 20 h. After concentration under vacuum, the residue was then purified by flash chromatography on silica

gel (CH_2Cl_2/MeOH: 95/5 to 85/15) to obtain the *N*-alkylpyridinium-indolizine **9** as a yellow solid in 50% yield.

^{1}H NMR (400MHz, CD_3OD) δ 9.81 (d, 1H, *J*=7.2 Hz), 8.88 (d, 2H, *J*=6.4 Hz), 8.16 (s, 1H), 8.04 (d, 2H, *J*=6.8 Hz), 7.85 (d, 2H, *J*=8.8 Hz), 7.78 (s, 1H), 7.20 (dd, 1H, *J*=7.2, 1.6 Hz), 7.13 (d, 2H, *J*=8.8, Hz), 4.72 (t, 2H, *J*=7.0 Hz), 3.95 (s, 3H), 3.91 (s, 3H), 3.63 (t, 2H, *J*=5.6 Hz), 3.46 (t, 2H, *J*=7.4 Hz), 3.32 (t, 2H, *J*=7.2 Hz), 2.21 (m, 2H); ^{13}C NMR (100 MHz, DMSO-d_6) δ183.3, 163.5, 162.2, 160.8, 144.3, 141.4, 139.0, 134.6, 132.2, 131.5, 130.9, 128.4, 127.7, 127.3, 121.9, 117.2, 117.0, 113.9, 104.0, 57.9, 57.1, 55.5, 51.1, 34.9, 34.2, 33.2; HRMS (ESI) m/z: calcd. for $C_{28}H_{29}N_2O_5$ $[M]^+$ 473.2071, obsd 473.2074 and calcd. for $C_{28}H_{30}N_2O_5$ $[M+H]^{2+}$ 237.1072, obsd 237.1071.

4.1.1.5 Dimethyl 7-[2-(4-pyridinyl)ethyl] indolizine-1,3-dicarboxylate **(6)**

This compound was prepared in two steps from 1,2-bis(4-pyridyl)ethane:

1) *N*-Alkylation

1,2-Bis(4-pyridyl)ethane (504 mg, 2.74 mmol) was dissolved in CH_3CN (15 mL). Methyl bromoacetate (0.9 eq.) was added and the solution was stirred at 70-80°C for 3 h. The white precipitate (dialkylated product) was removed by filtration. After concentration under vacuum, water was added then the aqueous solution was washed 4 times with AcOEt to remove the residual 1,2-bis(4-pyridyl)ethane. After aqueous phase concentration under vacuum, the residue was washed twice with CH_3CN. The organic solution was concentrated in vacuo to give an orange oil composed of a 4/1 mixture of 1-(2-methoxy-2-oxoethyl)-4-[2-(4-pyridinyl)ethyl]pyridinium bromide and 4,4'-(1,2-ethanediyl)bis[1-(2-methoxy-2-oxoethyl)pyridinium] dibromide in 30% yield. The mixture was directly used for the next step without purification.

2) Indolizine formation

The pyridinium mixture (145 mg, 0.43 mmol) and methyl propiolate (2.1 eq.) were dissolved in anh. CH_2Cl_2 (4 mL). NEt_3 (1.2 eq.) diluted in 1 mL of anh. CH_2Cl_2 was then added dropwise in the reacting mixture. After 2 h stirring at rt. water was added to the solution. The organic phase was separated and washed 2 more times with water and brine before being dried on $MgSO_4$ and concentrated under reduced pressure. The residue was then purified by flash chromatography on silica gel (CH_2Cl_2/MeOH: 98/2) to obtain indolizine **6** as an amorphous orange solid in 40% yield.

^{1}H NMR (400MHz, $CDCl_3$) δ 9.46 (dd, 1H, *J*=7.2, 0.8 Hz), 8.56 (dd, 2H, *J*=4.4, 1.6 Hz), 8.19 (d, 1H, *J*=0.8 Hz), 7.99 (s, 1H), 7.17 (dd, 2H, *J*=4.4, 1.6 Hz), 6.84 (dd, 1H, *J*=7.2, 2.0 Hz), 3.96 (s, 3H), 3.95 (s, 3H), 3.07 (m, 4H); ^{13}C NMR (100 MHz, $CDCl_3$) δ164.7, 161.6, 150.0, 149.5, 139.5, 139.4, 127.8 124.5, 123.8, 117.9, 115.9, 114.2, 104.2, 51.4, 51.2, 36.0, 35.8; HRMS (ESI) m/z: calcd. for $C_{19}H_{19}N_2O_4$ $[M+H]^+$ 339.1339, obsd 339.1338.

4.1.1.6 Dimethyl 7-[2-(1-methylpyridinium-4-yl)ethyl]indolizine-1,3-dicarboxylate iodide **(10)**

The indolizine **6** (42 mg, 0.12 mmol) was dissolved in CH_3CN (2 mL). Iodomethane (1.5 eq.) was added and the solution was stirred at 50°C for 2 h before adding another portion of iodomethane (1.5 eq.). After 2 h more stirring, the solution was concentrated under vacuum. The residue was then purified by flash chromatography on silica gel (CH_2Cl_2/MeOH: 96/4 to

90/10) to obtain the *N*-alkylpyridinium-indolizine **10** was thus isolated as a yellow solid in 85% yield.

^{1}H NMR (400MHz, $CDCl_3$) δ 9.49 (d, 1H, *J*=6.8 Hz), 9.10 (d, 2H, *J*=5.6 Hz), 8.12 (s, 1H), 7.99 (s, 1H), 7.93 (d, 2H, *J*=5.6 Hz), 6.92 (d, 1H, *J*=6.8 Hz), 4.67 (s, 3H), 3.96 (s, 3H), 3.95 (s, 3H), 3.39 (t, 2H, *J*=7.6 Hz), 3.22 (t, 2H, *J*=7.8 Hz); ^{13}C NMR (100 MHz, $CDCl_3$) δ164.6, 161.4, 161.1, 145.1, 138.9, 137.6, 128.3 128.0, 124.1, 117.9, 115.7, 114.5, 104.4, 51.5, 51.3, 49.0, 36.2, 34.9; HRMS (ESI) m/z: calcd. for $C_{20}H_{21}N_2O_4$ $[M]^+$ 353.1496, obsd 353.1497.

*4.1.2 **I**nd-PyC3 series*

4.1.2.1 Methyl 3-(p-methoxybenzoyl)-7-[3-(4-pyridinyl)propyl] indolizine-1-carboxylate **(11)**

This compound was prepared in two steps from 1,3-bis(4-pyridyl)propane

1) *N*-Alkylation

1,3-Bis(4-pyridyl)propane (676 mg, 3.4 mmol) was dissolved in CH_3CN (8 mL). 2-Bromo-*p*-methoxyacetophenone (1 eq.) was added and the solution was stirred at 70-80°C for 2 h. The white precipitate was filtrated and then purified by flash chromatography on silica gel (CH_2Cl_2/MeOH: 90/10). The 1-(2-(*4*-methoxyphenyl-2-oxoethyl)-4-[3-(4-pyridinyl)propyl]pyridinium bromide was thus isolated as a white solid in 41% yield (600 mg).

^{1}H NMR (400MHz, CD_3OD) δ8.76 (d, 2H, *J*=6.8 Hz), 8.49 (dd, 2H, *J*=4.8, 1.6 Hz), 8.13-8.08 (m, 4H), 7.40 (dd, 2H, *J*=4.8, 1.6 Hz), 7.17 (dd, 2H, *J*=6.8, 2.0 Hz), 3.97 (s, 3H), 3.11 (t, 2H, *J*=7.8 Hz), 2.87 (t, 2H, *J*=7.8 Hz), 2.21 (m, 2H); ^{13}C NMR (100 MHz, CD_3OD) δ188.2, 165.2, 163.7, 152.1, 148.6, 145.4, 130.5, 127.4, 127.3, 126.3, 124.3, 114.1, 54.9, 34.7, 34.0, 29.6; HRMS (ESI) m/z: calcd. for $C_{22}H_{23}N_2O_2$ $[M]^+$ 347.1754, obsd 347.1754 and calcd. for $C_{22}H_{24}N_2O_2$ $[M+H]^{2+}$ 174.0913, obsd 174.0917.

2) Indolizine formation

The pyridinium salt thus obtained (540 mg, 1.26 mmol) and methyl propiolate (2.2 eq.) were dissolved in anh. CH_2Cl_2 (10 mL). NEt_3 (1.2 eq.) diluted in 5 mL of anh. CH_2Cl_2 was then added dropwise in the reacting mixture. After 2 h stirring at rt, water was added to the solution. The organic phase was separated and washed 2 more times with water and brine before being dried on $MgSO_4$ and concentrated under reduced pressure. The residue was then purified by flash chromatography on silica gel (CH_2Cl_2/MeOH: 98/2) to obtain indolizine **11** in 68% yield.

^{1}H NMR (400MHz, $CDCl_3$) δ 9.74 (d, 1H, *J*=7.2 Hz), 8.44 (d, 2H, *J*=5.6 Hz), 8.10 (s, 1H), 7.75 (d, 2H, *J*=8.8 Hz), 7.71 (s, 1H), 7.06 (d, 2H, *J*=6.0 Hz), 6.93 (d, 2H, *J*=8.8 Hz), 6.83 (dd, 1H, *J*=7.2, 1.6 Hz), 3.82 (s, 6H), 2.71 (t, 2H, *J*=7.6 Hz), 2.62 (t, 2H, *J*=7.6 Hz), 1.99 (m, 4H); ^{13}C NMR (100 MHz, $CDCl_3$) δ184.4, 164.7, 162.6, 150.5, 149.8, 142.4, 140.2, 132.4, 131.2, 128.9, 128.6, 123.9, 122.5, 117.7, 116.5, 113.7, 104.7, 55.5, 51.2, 35.0, 34.6, 30.7; HRMS (ESI) m/z: calcd. for $C_{26}H_{25}N_2O_4$ $[M+H]^+$ 429.1809, obsd 429.1810.

4.1.2.2 Methyl 3-(p-methoxybenzoyl)-7-[3-(1-methylpyridinium-4-yl)propyl]indolizine-1-carboxylate iodide **(13)**

The indolizine **11** (102 mg, 0.24 mmol) was dissolved in CH_3CN (4 mL). Iodomethane (1.5 eq.) was added and the solution was stirred at 50°C for 4 h. After concentration under vacuum, the brown residue was washed with CH_2Cl_2. After drying, the *N*-alkylpyridinium-indolizine **13** was thus isolated as an orange solid with a quantitative yield.
^{1}H NMR (400MHz, $CDCl_3$) δ 9.71 (d, 1H, *J*=7.2 Hz), 9.04 (d, 2H, *J*=6.0 Hz), 8.08 (s, 1H), 7.83 (d, 2H, *J*=6.4 Hz), 7.75 (d, 2H, *J*=8.4 Hz), 7.70 (s, 1H), 6.93 (d, 2H, *J*=8.4, Hz), 6.90 (dd, 1H, *J*=7.2, 1.6 Hz), 4.57 (s, 3H), 3.83 (s, 3H), 3.82 (s, 3H), 2.91 (t, 2H, *J*=7.6 Hz), 2.79 (t, 2H, *J*=7.6 Hz), 2.08 (m, 2H); ^{13}C NMR (100 MHz, $CDCl_3$) δ184.4, 164.6, 162.6, 162.3, 145.0, 141.1, 139.9, 132.2, 131.2, 129.1, 128.5, 128.1, 122.6, 117.8, 116.4, 113.8, 104.9, 55.5, 51.3, 49.0, 35.1, 34.7, 30.0; HRMS (ESI) m/z: calcd. for $C_{27}H_{27}N_2O_4$ $[M]^+$ 443.1965, obsd 443.1966.

4.1.2.3 Methyl 3-(p-methoxybenzoyl)-7-[3-(1-[(3,5-dimethoxyphenyl)methyl]pyridinium-4-yl)propyl] indolizine-1-carboxylate bromide **(14)**

The indolizine **11** (193 mg, 0.45 mmol) was dissolved in CH_3CN (4 mL). 3,5-Dimethoxybenzyl bromide (1.2 eq.) was added and the solution was stirred at 70-80°C for 3 h. After concentration under vacuum, the brown residue was washed with CH_2Cl_2. After drying, the *N*-alkylpyridinium-indolizine **14** was thus isolated as a brown solid with a quantitative yield.
^{1}H NMR (400MHz, $CDCl_3$) δ 9.73 (d, 1H, *J*=7.2 Hz), 9.31 (d, 2H, *J*=6.4 Hz), 8.09 (s, 1H), 7.77-7.71 (m, 5H), 6.94 (dd, 2H, *J*=6.8, 2.0 Hz), 6.85 (d, 1H, *J*=7.2 Hz), 6.76 (d, 2H, *J*=2.0 Hz), 6.36 (dd, 1H, *J*=2.0 Hz), 6.04 (s, 2H), 3.83 (s, 3H), 3.82 (s, 3H), 3.71 (s, 6H), 2.85 (t, 2H, *J*=7.6 Hz), 2.77 (t, 2H, *J*=7.6 Hz), 2.04 (m, 2H); ^{13}C NMR (100 MHz, $CDCl_3$) δ184.4, 164.6, 162.6 162.2, 161.7, 144.4, 141.0, 139.9, 134.7, 132.3, 131.2, 129.1, 128.5, 127.8, 122.6, 117.7, 116.3, 113.8, 107.5, 104.9, 102.0, 63.8, 55.9, 55.5, 51.3, 35.1, 34.8, 29.8; HRMS (ESI) m/z: calcd. for $C_{35}H_{35}N_2O_6$ $[M]^+$ 579.2490, obsd 579.2495 and calcd. for $C_{35}H_{36}N_2O6$ $[M+H]^{2+}$ 290.1281, obsd 290.1279.

4.1.2.4 Dimethyl 7-[3-(4-pyridinyl)propyl]indolizine-1,3-dicarboxylate **(12)**
This compound was prepared in two steps from 1,3-bis(4-pyridyl)propane

1) *N*-Alkylation

1,3-Bis(4-pyridyl)propane (502 mg, 2.53 mmol) was dissolved in CH_3CN (5 mL). Methyl bromoacetate (0.9 eq.) was added and the solution was stirred at 70-80°C for 3 h. After concentration under vacuum, water was added then the aqueous solution was washed 4 times with CH_2Cl_2 to remove the residual 1,3-bis(4-pyridyl)propane. After aqueous phase concentration under vacuum, the residue was washed with cold CH_3CN. The organic solution was concentrated to give brown oil composed of a 10/1 mixture of 1-(2-methoxy-2-oxoethyl)-4-[3-(4-pyridinyl)propyl]pyridinium bromide and 4,4'-(1,3-propanediyl)bis[1-(2-methoxy-2-oxoethyl) pyridinium] dibromide in 55% yield. The mixture was directly used in the next step.

2) Indolizine formation

The pyridinium mixture (217 mg, 0.62 mmol) and methyl propiolate (2.1 eq.) were dissolved in anh. CH_2Cl_2 (5 mL). NEt_3 (1.2 eq.) diluted in 2 mL of anh. CH_2Cl_2 was then

added dropwise in the reacting mixture. After 4 h stirring at rt water was added to the solution. The organic phase was separated and washed 2 more times with water and brine before being dried on $MgSO_4$ and concentrated under reduced pressure. The residue was then purified by flash chromatography on silica gel (CH_2Cl_2/MeOH: 98/2) to obtain indolizine **12** as an amorphous orange solid in 55%.
^{1}H NMR (400MHz, $CDCl_3$) δ 9.43 (d, 1H, *J*=7.2 Hz), 8.52 (d, 2H, *J*=4.4 Hz), 8.16 (s, 1H), 7.96 (s, 1H), 7.15 (d, 2H, *J*=4.4 Hz), 6.85 (d, 1H, *J*=7.2 Hz), 3.93 (s, 6H), 2.77 (t, 2H, *J*=7.6 Hz), 2.71 (t, 2H, *J*=7.6 Hz), 2.07 (m, 2H); ^{13}C NMR (100 MHz, $CDCl_3$) δ164.7, 161.5, 150.6, 149.7, 140.5, 139.5, 127.7 124.5, 124.1, 123.9, 117.7, 115.9, 114.1, 104.0, 51.9, 51.3, 34.9, 34.6, 30.7; HRMS (ESI) m/z: calcd. for $C_{12}H_{21}N_2O_4$ $[M+H]^+$ 353.1496, obsd 353.1495.

4.1.2.5 Dimethyl 7-[3-(1-methylpyridinium-4-yl)propyl]indolizine-1,3-dicarboxylate iodide **(15)**
The indolizine **12** (50 mg, 0.14 mmol) was dissolved in CH_3CN (2 mL). Iodomethane (3 eq.) was added and the solution was stirred at 60°C for 3 h. After concentration under vacuum, the brown residue was washed with CH_2Cl_2 and Et_2O. After drying, the *N*-alkylpyridinium-indolizine **15** was thus isolated as a brownish solid (71%).
^{1}H NMR (400MHz, $CDCl_3$) δ 9.46 (d, 1H, *J*=7.2 Hz), 9.15 (d, 2H, *J*=6.4 Hz), 8.15 (s, 1H), 7.98 (s, 1H), 7.93 (d, 2H, *J*=6.4 Hz), 6.93 (d, 1H, *J*=7.2 Hz), 4.68 (s, 3H), 3.95 (s, 6H), 3.02 (t, 2H, *J*=7.6 Hz), 2.87 (t, 2H, *J*=7.6 Hz), 2.18 (m, 2H); ^{13}C NMR (100 MHz, $CDCl_3$) δ164.7, 162.3, 161.5, 145.0, 139.3, 128.0 127.9, 124.5, 117.9, 115.9, 114.3, 104.2, 51.5, 51.3, 49.0, 35.1, 34.6, 30.0; HRMS (ESI) m/z: calcd. for $C_{21}H_{23}N_2O_4$ $[M]^+$ 367.1652, obsd 367.1651.

4.1.2.6 Dimethyl 7-[3-(1-[(3,5-dimethoxyphenyl)methyl]pyridinium-4-yl)propyl]indolizine1,3-dicarboxylate bromide **(16)**
The indolizine **12** (58 mg, 0.14 mmol) was dissolved in CH_3CN (2 mL). 3,5-Dimethoxybenzyl bromide (1.1 eq.) was added and the solution was stirred at 70°C for 3 h. After concentration under vacuum, the brown residue was washed with CH_2Cl_2 and Et_2O. After drying, the *N*-alkylpyridinium-indolizine **16** was thus isolated as a brownish solid in 90% yield.
^{1}H NMR (400MHz, $CDCl_3$) δ 9.47 (d, 1H, *J*=7.2 Hz), 9.43 (d, 2H, *J*=5.6 Hz), 8.16 (s, 1H), 7.98 (s, 1H), 7.83 (d, 2H, *J*=5.6 Hz), 6.88 (m, 3H), 6.48 (s, 1H), 6.15 (s, 2H), 3.96 (s, 6H), 3.83 (s, 6H), 2.95 (t, 2H, *J*=7.6 Hz), 2.85 (t, 2H, *J*=7.6 Hz), 2.13 (m, 2H); ^{13}C NMR (100 MHz, $CDCl_3$) δ164.7, 162.3, 161.7, 161.5, 144.4, 139.3, 139.2, 134.6, 128.0 127.8, 124.5, 117.8, 115.7, 114.4, 107.5, 107.0, 104.2, 102.0, 63.7, 55.9, 55.4, 51.4, 51.2, 35.1, 34.7, 29.8; HRMS (ESI) m/z: calcd. for $C_{29}H_{31}N_2O_6$ $[M]^+$ 503.2177, obsd 503.2179.

4.1.3 Bis-pyridinium salts

4.1.3.1 1-Methyl-4-[2-[1-(2-methoxy-2-oxoethyl)pyridinium-4-yl]ethyl]pyridinium bromide and iodide **(18)**
1-Methyl-4-[2-(4-pyridinyl)ethyl]-pyridinium iodide [64] (315 mg, 0.97 mmol) was dissolved in CH_3CN (7 mL). Methyl bromoacetate (3 eq.) was added and the solution was

stirred at 70-80°C for 20 h. After concentration under vacuum, the residue was washed 3 times with CH_2Cl_2. After drying, the bi-pyridinium **18** was thus isolated as a brown solid in 20% yield (246 mg).
^{1}H NMR (400MHz, CD_3OD) δ8.89 (d, 2H, *J*=6.8 Hz), 8.84 (d, 2H, *J*=6.8 Hz), 8.17 (d, 2H, *J*=6.8 Hz), 8.08 (d, 2H, *J*=6.8 Hz), 5.59 (s, 2H), 4.40 (s, 3H), 3.89 (s, 3H), 3.49 (m, 4H); ^{13}C NMR (100 MHz, D_20) δ168.0, 162.3, 160.0, 145.4, 144.8, 128.1, 127.9, 125.8, 60.3, 54.0, 47.6, 34.4, 34.1; HRMS (ESI) m/z: calcd. for $C_{16}H_{19}N_2O_2$ $[M\text{-}H]^+$ 271.1441, obsd 271.1440 and calcd. for $C_{16}H_{20}N_2O_2$ $[M]^{2+}$ 136.0767, obsd 136.0759.

4.1.3.2 1-[2-(4-Methoxyphenyl)-2-oxoethyl]-4-[3-(1-methylpyridinium-4-yl)propyl] pyridinium iodide and bromide **(19)**
1-Methyl-4-[3-(4-pyridinyl)propyl]-pyridinium iodide [65] (238 mg, 0.7 mmol) was dissolved in CH_3CN (8 mL). 2-Bromo-*p*-methoxyacetophenone (3 eq.) was added and the solution was stirred at 70-80°C for 20 h. After concentration under vacuum, the residue was washed 3 times with CH_2Cl_2. After drying, the bi-pyridinium **19** was thus isolated as a brown solid in 93% yield.
^{1}H NMR (400MHz, CD_3OD) δ8.81 (d, 2H, *J*=6.4 Hz), 8.78 (d, 2H, *J*=6.8 Hz), 8.13 (d, 2H, *J*=6.4 Hz), 8.11 (d, 2H, *J*=9.2 Hz), 8.04 (d, 2H, *J*=6.4 Hz), 7.15 (d, 2H, *J*=8.8 Hz), 4.40 (s, 3H), 3.95 (s, 3H), 3.15 (m, 4H), 2.30 (m, 2H); ^{13}C NMR (100 MHz, D_2O) δ190.8, 163.8, 164.4, 162.1, 145.3, 144.6, 131.3, 128.0, 126.2, 114.8, 56.1, 47.7, 34.8, 34.5, 28.5; HRMS (ESI) m/z: calcd. for $C_{23}H_{25}N_2O_2$ $[M\text{-}H]^+$ 361.1911, obsd 361.1912 and calcd. for $C_{23}H_{26}N_2O_2$ $[M]^{2+}$ 181.0992, obsd 181.0996.

4.1.3.3 1-Methyl-4-[3-[1-(2-methoxy-2-oxoethyl)pyridinium-4-yl]propyl]pyridinium bromide and iodide **(20)**
1-Methyl-4-[2-(4-pyridinyl)propyl]-pyridinium iodide [65] (216 mg, 0.63 mmol) was dissolved in CH_3CN (5 mL). Methyl bromoacetate (2 eq.) was added and the solution was stirred at 70-80°C for 5 h. After concentration under vacuum, the residue was washed 3 times with CH_2Cl_2. After drying, the bi-pyridinium **20** was thus isolated as a brown solid in 80% yield (246 mg).
^{1}H NMR (400MHz, CD_3OD) δ8.89 (d, 2H, *J*=6.8 Hz), 8.83 (d, 2H, *J*=6.8 Hz), 8.15 (d, 2H, *J*=6.8 Hz), 8.06 (d, 2H, *J*=6.8 Hz), 5.61 (s, 2H), 4.42 (s, 3H), 3.91 (s, 3H), 3.15 (m, 4H), 2.29 (m, 2H); ^{13}C NMR (100 MHz, D_2O) δ168.2, 164.4, 162.1, 145.2, 144.6, 128.8, 128.0, 125.2, 60.4, 54.2, 47.7, 34.8, 34.5, 28.5; HRMS (ESI) m/z: calcd. for $C_{17}H_{21}N_2O_2$ $[M\text{-}H]^+$ 285.1598, obsd 285.1597 and calcd. for $C_{17}H_{22}N_2O_2$ $[M]^{2+}$ 143.0835, obsd 143.0838.

4.2 Biological evaluation

4.2.1 Antioxidant activity: DPPH assay

In a 96-well plate, 100 µL of a 100 µg/mL DPPH methanolic solution were added to 100 µL samples at concentrations ranging from 100 to 1500 µg/mL in methanol. The resulting solutions were then homogenized and left in the dark at rt for 35 min. The absorbance values at 517 nm were recorded after this time period. The blank sample used was a 1:1 mixture of methanol and DPPH solution. A 48 µg/mL solution of rutin was used as a reference standard.

The DPPH inhibition percentage, which relates to the antioxidant activity of rutin or of the tested compounds, was calculated using the following formula: % inhibition = (A_{blank} – A_{sample})/A_{blank} *100. The assays were performed in triplicates. The initial solutions of samples were prepared by dilution of 20 mM stock DMSO solutions with MeOH to reach the concentration of 3 mg/mL. For all tested compounds, the highest concentration in well was 0.75 mg/mL.

4.2.2 Cholinesterase inhibition assays

Acetylcholinesterase ((E.C. 3.1.1.7) from Electrophorus electricus (eeAChE), Type V-S, (Sigma C2888) ≥1000U/mg protein; Butyrylcholinesterase (E.C. 3.1.1.8) from equine serum (eqBChE) (Sigma ref C1057), ≥900U/mg protein; Human acetylcholinesterase, recombinant, expressed in HEK 293 cells, lyophilized powder, (ref Sigma C1682), ≥1000U/mg protein; Human butyrylcholinesterase (hBChE) from human serum (ref Sigma B4186), 4U/vial; 5,5'-dithiobis-(2- nitrobenzoic acid) (Ellman's reagent, DTNB), S-acetylthiocholine iodide (ATCI), S-butyrylthiocholine iodide, and donepezil hydrochloride were purchased from Sigma Aldrich.

The experimental procedure described below for AChE was also applied to BChE by replacing the S-acetylthiocholine by the S-butyrylthiocholine.
AChE solution was prepared in Tris·HCl buffer (pH=8; 50 mM, with BSA (Bovine serum albumine) 0.1% w), and then diluted at an activity of 0.27U for non-symmetrical hybrids (the dilution was 0.5U for the symmetrical bis-pyridinium salts and bis-indolizines **1'-4'** series, see Table S4). S-Acetylthiocholine iodide solution was prepared in ultrapure water, at the concentration of 15 mM. DTNB (5,5`-dithiobis(2-nitrobenzoic acid)) was diluted in phosphate buffer (pH=7.4; 1.5 mM).
The test solutions were prepared at a concentration of 20 mM (stock solutions in DMSO) and then diluted with Tris·HCl buffer (pH=8.0, 50 mM, 0.1M NaCl, 0.02M $MgCl_2$), freshly prepared solutions were used for assays performed in the same day.
In 96-well plates, 160 µL of 1.5mM DTNB solution and 50 µL of AChE (0.5 or 0.27U/mL) solutions were incubated with 10 µL of various concentrations of the tested compounds (final concentrations in wells were 100 to 0.04 µM (compared to 20 to 0.05 µM for the symmetrical compounds, Table S4) at 37 °C, and then 30 µL of acetylthiocholine iodide (15 mM) were added. The absorbance was measured at 48s intervals for minimum 20 cycles at 405 nm wavelength with the Omega fluorescence plate reader (BMG LABTECH GmbH, Offenburg, Germany). IC_{50} values were obtained by plotting the initial velocities versus the concentrations of the tested compounds and using nonlinear regression analysis of the dose-response - inhibition ([inhibitor] *vs* response, 3 parameters) curve. Results were expressed as the mean ± SD of at least three different experiments performed in triplicate. The blanks contained no enzyme solution, its volume being replaced by ultrapure water [14].

4.2.3 Molecular docking calculations

All modelling calculations were performed with the Schrödinger Suite version 2017-4.
4.2.3.1 Protein preparation
The crystal structures of the complexes of hAChE with dihydrotanshinone I (PDB ID: 4M0E[66], solved at 2 Å resolution) and of hBChE with (S)-2-(butylamino)-*N*-(2-cycloheptylethyl)-3-(1*H*-indol-3-yl) propanamide (PDB ID:6QAA, solved at 1.9 Å) [67], were used for the docking calculations. The proteins were prepared using the Protein

Preparation Wizard tool [68]. Missing side-chains were built and water molecules were retrieved. The partial atomic charges were derived from the OPLS3 force field [69]. Hydrogen atoms were added considering the pH7 value and using the algorithm PropKa [70]. The orientation of the asparagine and glutamine side-chains were performed so as to maximize the hydrogen bond network. An all-atom energy minimization with a 0.3 Å heavy-atom RMSD criteria for termination was performed using the Impref utility [71] and OPLS3.

4.2.3.2 Ligand preparation

The low-energy conformers of the compounds were generated using the LigPrep module[72]. The ligands were docked flexibly; the parameters for van der Waals radii were scaled by 0.80 for atoms with partial charges less than 0.15e, and non-planar amide bonds were penalized. Relevant ionization and tautomeric states at pH comprised between 5 and 9 were generated using the Hammett and Taft methodology implemented in Epik [73]. The resulting conformations were energy-minimized using OPLS3 force field [69] and a maximum of 100 conformations per ligand were generated and subjected to post-docking minimization.

4.2.3.3 Docking calculations

The Glide algorithm version 7.7 [74], [75] in Standard precision mode with the OPLS3 force field was used. The receptors were considered as rigid, but the hydroxyls of Ser, Thr and Tyr residues were allowed to rotate, including residue Y337, known to adopt different conformers depending on the ligand that is co-crystallized [76]. A large receptor grid encompassing both the catalytic site and the peripheral site was generated for both enzymes. We used a scaling of van der Waals radii of 1 for atoms with partial charges less than 0.25e. The shape and physico-chemical properties of the binding sites were mapped onto grids defined with large dimensions to reflect the presence of the two main binding sites. The dimensions of the receptor grids were respectively 36*42*35 $Å^3$ and 31*35*30 $Å^3$ for respectively the hAChE and hBChE enzymes, centered on the co-crystallized ligand. Our docking procedure was validated as it was able to recover the binding pose of dihydrotanshinone I in hAChE with a RMSD of 0.017Å.

4.2.4 Study on amyloid fibers

The AcPHF6 (Ac-VQIVYK-NH_2) peptide was prepared as previously described [46]. The AcR3 peptide corresponds to G271-G323ΔR2 tau fragment and was synthesized by Fmoc/tBu strategy on Rink amide MBHA resin.

4.2.4.1 Thioflavin T fluorescence assays

A typical ThT assay's microplate includes ThT control wells, peptide (AcPHF6 or R3) control wells and **Ind-PyCx** control wells. The wells were prepared in hexaplicate. The total volume of each well was 100 µL for a final concentration of 100 µM peptide, 10 µM ThT, 10 µM heparin (for AcR3) and 100 µM **Ind-PyCx** with a maximum of 0.5 % DMSO in 50 mM phosphate buffer pH 7.4. In blank wells, the peptide solution above was replaced by pure water. The assays were conducted in standard 96-well plates (U-shape, black, polypropylene, Greiner Bio-One, USA) in a POLARstar Omega fluorescence plate reader (BMG LABTECH GmbH, Offenburg, Germany) at room temperature (AcPHF6 peptide) or 37 °C (AcR3 peptide) with excitation and emission wavelengths at 440 nm and 480 nm, respectively. Fluorescence data were recorded every minute over 2 h (AcPHF6 peptide) or over 34 h (AcR3 peptides) with 10 s shaking (700 rpm) prior to each reading (top optic, orbital averaging of 3 mm diameter) with a gain of 1200. Inhibitions reported in Figure 6 are

calculated from the average of the hexaplicate, and the errors represent the SEM of three independent experiments performed in hexaplicates.

4.2.4.2 Absorption spectra

Absorption spectra were acquired on a spectrophotometer UV-1650 PC Shimadzu using an optical length of 10 mm. Acquisitions were recorded from 200 nm to 600 nm. Samples were prepared to give a final concentration of 100 µM **Ind-PyCx** with a maximum of 0.5 % DMSO in 50 mM phosphate buffer pH 7.4.

4.2.4.3 Emission spectra

Emission spectra were acquired on a FluoroMax4 Horiba Spectrometer a quartz cell with a 3 mm path length and a maximum volume of 300 µL.

Emission spectra of **Ind-PyCx** series alone were recorded from 100 µM **Ind-PyCx** alone in 50 mM phosphate buffer pH 7.4 with a maximum of 0.5% DMSO. Their emission spectra in presence of pre-formed fibers were recorded after adding the **Ind-PyCx** solution in 50 mM phosphate buffer pH 7.4 (0.5 % DMSO) to preformed AcPHF6 fibers (or AcR3 fibers) in presence or without ThT. The final concentration of **Ind-PyCx** compounds in cell was 100 µM. AcPHF6 pre-formed fibers were prepared in an Eppendorf® Protein LoBind tube by incubating 100 µM AcPHF6 peptide in phosphate buffer for 24 h at room temperature in absence or in presence of 10 µM ThT (for the displacement assay). For AcR3 pre-formed fibers, they were prepared in an Eppendorf® Protein LoBind tube by incubating 100 µM AcR3 peptide and 10 µM heparin in phosphate buffer for 24 h at 37°C in absence or presence of 10 µM ThT (for the displacement assay).

4.2.4.4 Circular Dichroism

CD spectra were acquired on a JASCO J-810 spectropolarimeter (Jasco Corporation, Tokyo, Japan) using a quartz cell with a 1 mm path length and a maximum volume of 300 µL. Acquisitions were recorded at room temperature between 260 nm and 206 nm with a spectral resolution of 1 nm, an average time of 1 s per data point and a band width of 10 nm. The spectra reported represent an average of four acquisitions and have not be smoothed. The total volume of each quartz cell was 300 µL for a final concentration of 100 µM AcR3, 10 µM heparin and 100 µM **Ind-PyCx** in 50 mM phosphate buffer pH 7.4 with a maximum of 0.5 % DMSO. Prior to the acquisitions in the quartz cell, the mixtures were incubated at 37°C for 24 h in an Eppendorf® Protein LoBind tube.

5. Acknowledgments

This work has been partially supported by Labex Arcane, CBH-EUR-GS (ANR-17-EURE-0003), by the PolyNatCarnot Institute (Investissements d'Avenir -grant agreement n°ANR-11-CARN-007-01), by NeuroCoG IDEX UGA in the framework of the "Investissements d'avenir" program (ANR-15-IDEX-02), and by a grant of the Romanian National Authority for Scientific Reasearch and Innovation (CNCS-UEFISCDI, PN-II-ID-PCE-2011-3-0226, CCCDI-UEFISCDI, project number 85BM/2017). The NanoBio ICMG (UAR 2607) is acknowledged for providing facilities for mass spectrometry analyses (A. Durand, L. Fort, R. Gueret) and for NMR analyses (M.-C. Molina).

6. References and notes

[1] S. Small, R. Mayeux, Alzheimer's disease and related dementias, Merrit's Neurology 107 (2005) 771-6.
[2] J. Cummings, G. Lee, A. Ritter, M. Sabbagh, K. Zhong, Alzheimer's disease drug development pipeline: 2019, Alzheimer's Dement. 5 (2019) 272-293.
[3] P. Anand, B. Singh, A review on cholinesterase inhibitors for Alzheimer's disease, Arch. Pharm. Res. 36(4) (2013) 375-399.
[4] M. de Freitas Silva, K.S. Dias, V.S. Gontijo, C.J.C. Ortiz, J. Viegas, Multi-target directed drugs as a modern approach for drug design towards Alzheimer's disease: an update, Curr. Med. Chem. 25(29) (2018) 3491-3525.
[5] R. Leon, A.G. Garcia, J. Marco-Contelles, Recent advances in the multitarget-directed ligands approach for the treatment of Alzheimer's disease, Med. Res. Rev. 33(1) (2013) 139-189.
[6] P. Mishra, A. Kumar, G. Panda, Anti-cholinesterase hybrids as multi-target-directed ligands against Alzheimer's disease (1998–2018), Bioorg. Med. Chem. 27(6) (2019) 895-930.
[7] S. Montanari, M. Bartolini, P. Neviani, F. Belluti, S. Gobbi, L. Pruccoli, A. Tarozzi, F. Falchi, V. Andrisano, P. Miszta, A. Cavalli, S. Filipek, A. Bisi, A. Rampa, Multitarget Strategy to Address Alzheimer's Disease: Design, Synthesis, Biological Evaluation, and Computational Studies of Coumarin-Based Derivatives, ChemMedChem 11(12) (2016) 1296-1308.
[8] C.J.C. Ortiz, M. de Freitas Silva, V.S. Gontijo, F.P.D. Viegas, K.S.T. Dias, C. Viegas, Design of Multi-target Directed Ligands as a Modern Approach for the Development of Innovative Drug Candidates for Alzheimer's Disease, Methods in Pharmacology and Toxicology, Springer Science, New-York, 2018, pp. 255-351.
[9] T. Wang, X.-h. Liu, J. Guan, S. Ge, M.-B. Wu, J.-p. Lin, L.-r. Yang, Advancement of multi-target drug discoveries and promising applications in the field of Alzheimer's disease, Eur. J. Med. Chem. 169 (2019) 200-223.
[10] P. Zhang, S. Xu, Z. Zhu, J. Xu, Multi-target design strategies for the improved treatment of Alzheimer's disease, Eur. J. Med. Chem. 176 (2019) 228-247.
[11] M. Singh, M. Kaur, N. Chadha, O. Silakari, Hybrids: a new paradigm to treat Alzheimer's disease, Mol. Divers. 20(1) (2016) 271-297.
[12] M. Alipour, M. Khoobi, A. Foroumadi, H. Nadri, A. Moradi, A. Sakhteman, M. Ghandi, A. Shafiee, Novel coumarin derivatives bearing *N*-benzyl pyridinium moiety: potent and dual binding site acetylcholinesterase inhibitors, Bioorg. Med. Chem. 20(24) (2012) 7214-7222.
[13] F. Baharloo, M.H. Moslemin, H. Nadri, A. Asadipour, M. Mahdavi, S. Emami, L. Firoozpour, R. Mohebat, A. Shafiee, A. Foroumadi, Benzofuran-derived benzylpyridinium bromides as potent acetylcholinesterase inhibitors, Eur. J. Med. Chem. 93 (2015) 196-201.
[14] J.-S. Lan, T. Zhang, Y. Liu, J. Yang, S.-S. Xie, J. Liu, Z.-Y. Miao, Y. Ding, Design, synthesis and biological activity of novel donepezil derivatives bearing *N*-benzyl pyridinium moiety as potent and dual binding site acetylcholinesterase inhibitors, Eur. J. Med. Chem. 133 (2017) 184-196.
[15] R. Palin, J.K. Clark, P. Cowley, A.W. Muir, E. Pow, A.B. Prosser, R. Taylor, M.-Q. Zhang, Novel piperidinium and pyridinium agents as water-soluble acetylcholinesterase inhibitors for the reversal of neuromuscular blockade, Bioorg. Med. Chem. Lett. 12(18) (2002) 2569-2572.

[16] F. Vafadarnejad, E. Karimpour-Razkenari, B. Sameem, M. Saeedi, O. Firuzi, N. Edraki, M. Mahdavi, T. Akbarzadeh, Novel *N*-benzylpyridinium moiety linked to arylisoxazole derivatives as selective butyrylcholinesterase inhibitors: Synthesis, biological evaluation, and docking study, Bioorg. Chem. 92 (2019) 103192.
[17] M. Khoobi, M. Alipour, A. Sakhteman, H. Nadri, A. Moradi, M. Ghandi, S. Emami, A. Foroumadi, A. Shafiee, Design, synthesis, biological evaluation and docking study of 5-oxo-4, 5-dihydropyrano [3, 2-c] chromene derivatives as acetylcholinesterase and butyrylcholinesterase inhibitors, Eur. J. Med. Chem. 68 (2013) 260-269.
[18] H. Akrami, B.F. Mirjalili, M. Khoobi, H. Nadri, A. Moradi, A. Sakhteman, S. Emami, A. Foroumadi, A. Shafiee, Indolinone-based acetylcholinesterase inhibitors: synthesis, biological activity and molecular modeling, Eur. J. Med. Chem. 84 (2014) 375-381.
[19] M. Mollazadeh, M. Mohammadi-Khanaposhtani, A. Zonouzi, H. Nadri, Z. Najafi, B. Larijani, M. Mahdavi, New benzyl pyridinium derivatives bearing 2, 4-dioxochroman moiety as potent agents for treatment of Alzheimer's disease: Design, synthesis, biological evaluation, and docking study, Bioorg. Chem. 87 (2019) 506-515.
[20] S. Sowmiah, J.M. Esperança, L.P. Rebelo, C.A. Afonso, Pyridinium salts: from synthesis to reactivity and applications, Org. Chem. Front. 5(3) (2018) 453-493.
[21] P. Sharma, P. Srivastava, A. Seth, P.N. Tripathi, A.G. Banerjee, S.K. Shrivastava, Comprehensive review of mechanisms of pathogenesis involved in Alzheimer's disease and potential therapeutic strategies, Prog. Neurobiol. 174 (2019) 53-89.
[22] I.O. Ghinea, R.M. Dinica, Breakthroughs in Indole and Indolizine Chemistry–New Synthetic Pathways, New Applications, Scope of Selective Heterocycles from Organic and Pharmaceutical Perspective, IntechOpen, eBook, 2016.
[23] V. Sharma, V. Kumar, Indolizine: a biologically active moiety, Med. Chem. Res. 23(8) (2014) 3593-3606.
[24] M. Arvin-Berod, A. Desroches-Castan, S. Bonte, S. Brugière, Y. Coute, L. Guyon, J.-J. Feige, I. Baussanne, M. Demeunynck, Indolizine-based scaffolds as efficient and versatile tools: Application to the synthesis of biotin-tagged antiangiogenic drugs, ACS omega 2(12) (2017) 9221-9230.
[25] S.-K. Choi, J. Rho, S.E. Yoon, J.-H. Seok, H. Kim, J. Min, W. Yoon, S. Lee, H. Yun, O.-P. Kwon, Full Color Tunable Aggregation-Induced Emission Luminogen for Bioimaging Based on an Indolizine Molecular Framework, Bioconjug. Chem. 31(11) (2020) 2522-2532.
[26] D. Kim, J.H. Lee, H.Y. Kim, J. Shin, K. Kim, S. Lee, J. Park, J. Kim, Y. Kim, Fluorescent indolizine derivative YI-13 detects amyloid-β monomers, dimers, and plaques in the brain of 5XFAD Alzheimer transgenic mouse model, PloS one 15(12) (2020) e0243041.
[27] J. Sung, Y. Lee, J.-H. Cha, S.B. Park, E. Kim, Development of fluorescent mitochondria probe based on 1, 2-dihydropyrrolo [3, 4-b] indolizine-3-one, Dyes Pigments 145 (2017) 461-468.
[28] N.-L. Marangoci, L. Popovici, E.-L. Ursu, R. Danac, L. Clima, C. Cojocaru, A. Coroaba, A. Neamtu, I. Mangalagiu, M. Pinteala, A. Rotaru, Pyridyl-indolizine derivatives as DNA binders and pH-sensitive fluorescent dyes, Tetrahedron 72(50) (2016) 8215-8222.
[29] X. Zheng, R. Ji, X. Cao, Y. Ge, FRET-based ratiometric fluorescent probe for Cu^{2+} with a new indolizine fluorophore, Anal. Chim. Acta 978 (2017) 48-54.
[30] W.E. Meador, S.A. Autry, R.N. Bessetti, J.N. Gayton, A.S. Flynt, N.I. Hammer, J.H. Delcamp, Water-soluble NIR absorbing and emitting indolizine cyanine and indolizine squaraine dyes for biological imaging, J. Org. Chem. 85(6) (2020) 4089-4095.
[31] H. Chakravarty, Y. Ju, W.H. Chen, K.Y. Tam, Dual targeting of cholinesterase and amyloid beta with pyridinium/isoquinolium derivatives, Drug Dev. Res. 81(2) (2020) 242-255.

[32] M. Abdullaha, V.K. Nuthakki, S.B. Bharate, Discovery of methoxy-naphthyl linked *N*-(1-benzylpiperidine) benzamide as a blood-brain permeable dual inhibitor of acetylcholinesterase and butyrylcholinesterase, Eur. J. Med. Chem. 207 (2020) 112761.
[33] V. Hrabcova, J. Korabecny, B. Manyova, L. Matouskova, T. Kucera, R. Dolezal, K. Musilek, L. Gorecki, E. Nepovimova, K. Kuca, Bis-isoquinolinium and bis-pyridinium acetylcholinesterase inhibitors: in vitro screening of probes for novel selective insecticides, RSC Adv. 7(62) (2017) 39279-39291.
[34] R. Azzouz, L. Peauger, V. Gembus, M.-L. Ţînţaş, J. Sopková-de Oliveira Santos, C. Papamicaël, V. Levacher, Novel donepezil-like N-benzylpyridinium salt derivatives as AChE inhibitors and their corresponding dihydropyridine "bio-oxidizable" prodrugs: Synthesis, biological evaluation and structure-activity relationship, Eur. J. Med. Chem. 145 (2018) 165-190.
[35] F. Hosseini, A. Ramazani, M. Mohammadi-Khanaposhtani, M.B. Tehrani, H. Nadri, B. Larijani, M. Mahdavi, Design, synthesis, and biological evaluation of novel 4-oxobenzo [d] 1, 2, 3-triazin-benzylpyridinum derivatives as potent anti-Alzheimer agents, Bioorg. Med. Chem. 27(13) (2019) 2914-2922.
[36] M. Singh, M. Kaur, H. Kukreja, R. Chugh, O. Silakari, D. Singh, Acetylcholinesterase inhibitors as Alzheimer therapy: from nerve toxins to neuroprotection, Eur. J. Med. Chem. 70 (2013) 165-188.
[37] O.B. Østby, B. Dalhus, L.L. Gundersen, F. Rise, A. Bast, G.R. Haenen, Synthesis of 1-Substituted 7-Cyano-2, 3-diphenylindolizines and Evaluation of Antioxidant Properties, Eur. J. Org. Chem. 2000(22) (2000) 3763-3770.
[38] L.-L. Gundersen, K.E. Malterud, A.H. Negussie, F. Rise, S. Teklu, O.B. Østby, Indolizines as novel potent inhibitors of 15-lipoxygenase, Bioorg. Med. Chem. 11(24) (2003) 5409-5415.
[39] G. Ghotbi, M. Mahdavi, Z. Najafi, F.H. Moghadam, M. Hamzeh-Mivehroud, S. Davaran, S. Dastmalchi, Design, synthesis, biological evaluation, and docking study of novel dual-acting thiazole-pyridiniums inhibiting acetylcholinesterase and β-amyloid aggregation for Alzheimer's disease, Bioorg. Chem. 103 (2020) 104186.
[40] S. Abdpour, L. Jalili-Baleh, H. Nadri, H. Forootanfar, S.N.A. Bukhari, A. Ramazani, S.E.S. Ebrahimi, A. Foroumadi, M. Khoobi, Chromone derivatives bearing pyridinium moiety as multi-target-directed ligands against Alzheimer's disease, Bioorg. Chem. 110 (2021) 104750.
[41] M. Ahmed, J.B.T. Rocha, C.M. Mazzanti, A.L. Morsch, D. Cargnelutti, M. Corrêa, V. Loro, V.M. Morsch, M.R. Schetinger, Malathion, carbofuran and paraquat inhibit Bungarus sindanus (krait) venom acetylcholinesterase and human serum butyrylcholinesterase in vitro, Ecotoxicol. 16(4) (2007) 363.
[42] P. Kapková, V. Alptüzün, P. Frey, E. Erciyas, U. Holzgrabe, Search for dual function inhibitors for Alzheimer's disease: Synthesis and biological activity of acetylcholinesterase inhibitors of pyridinium-type and their Aβ fibril formation inhibition capacity, Bioorg. Med. Chem. 14(2) (2006) 472-478.
[43] Y. Seto, T. Shinohara, Structure-activity relationship of reversible cholinesterase inhibitors including paraquat, Arch. Toxicol. 62(1) (1988) 37-40.
[44] B. Furdui, R. Dinica, M. Demeunynck, I. Druta, A. Vlahovici, New reactive pyridinium-indolizines fluorophores, Rev. Roum. Chim. 52(7) (2007) 633-637.
[45] B. Furdui, R. Dinica, I.I. Druta, M. Demeunynck, Improved synthesis of cationic pyridinium-substituted indolizines, Synthesis 2006(16) (2006) 2640-2642.
[46] L. Lunven, H. Bonnet, S. Yahiaoui, W. Yi, L.n. Da Costa, M. Peuchmaur, A. Boumendjel, S. Chierici, Disruption of fibers from the tau model AcPHF6 by naturally occurring aurones and synthetic analogues, ACS Chem. Neurosci. 7(7) (2016) 995-1003.

[47] T. Mohamed, T. Hoang, M. Jelokhani-Niaraki, P.P. Rao, Tau-derived-hexapeptide 306VQIVYK311 aggregation inhibitors: nitrocatechol moiety as a pharmacophore in drug design, ACS Chem. Neurosci. 4(12) (2013) 1559-1570.
[48] J. Zheng, C. Liu, M.R. Sawaya, B. Vadla, S. Khan, R.J. Woods, D. Eisenberg, W.J. Goux, J.S. Nowick, Macrocyclic β-sheet peptides that inhibit the aggregation of a tau-protein-derived hexapeptide, J. Am. Chem. Soc. 133(9) (2011) 3144-3157.
[49] W.J. Goux, L. Kopplin, A.D. Nguyen, K. Leak, M. Rutkofsky, V.D. Shanmuganandam, D. Sharma, H. Inouye, D.A. Kirschner, The formation of straight and twisted filaments from short tau peptides, J. Biol. Chem. 279(26) (2004) 26868-26875.
[50] H. Kalász, S. Nurulain, G. Veress, S. Antus, F. Darvas, E. Adeghate, A. Adem, F. Hashemi, K. Tekes, Mini review on blood–brain barrier penetration of pyridinium aldoximes, J. Appl. Toxicol. 35(2) (2015) 116-123.
[51] A. Tsuji, Small molecular drug transfer across the blood-brain barrier via carrier-mediated transport systems, NeuroRx 2(1) (2005) 54-62.
[52] T.T. Wager, R.Y. Chandrasekaran, X. Hou, M.D. Troutman, P.R. Verhoest, A. Villalobos, Y. Will, Defining desirable central nervous system drug space through the alignment of molecular properties, in vitro ADME, and safety attributes, ACS Chem. Neurosci. 1(6) (2010) 420-434.
[53] H. Pajouhesh, G.R. Lenz, Medicinal chemical properties of successful central nervous system drugs, NeuroRx 2(4) (2005) 541-553.
[54] The bis-pyridinium di-cations **17-20** (and their symmetrical analogs **1'a-c** and **2'a-c**, see Table S4) are too polar (strongly negative LogP). It is also interesting to notice that the bis-indolizines (7,7'-bis-indolizines **3'a-c** and bis(indolizin-7-yl)ethane **4'a-c**) do not in general follow the rules as they are too lipophilic (LogP > 6), showing both high MW and PSA values (see Table S4). Their calculated high lipophilicity is experimentally correlated to a low solubility in water with formation of aggregates
[55] G.L. Ellman, K.D. Courtney, V. Andres, R.M. Featherstone, A new and rapid colorimetric determination of acetylcholinesterase activity, Biochem. Pharmacol. 7(2) (1961) 88-95.
[56] Q. Shen, B. Zhang, R. Xu, Y. Wang, X. Ding, P. Li, Antioxidant activity in vitro of the selenium-contained protein from the Se-enriched Bifidobacterium animalis 01, Anaerobe 16(4) (2010) 380-386.
[57] H. Levine III, Thioflavine T interaction with synthetic Alzheimer's disease β-amyloid peptides: Detection of amyloid aggregation in solution, Protein Sci. 2(3) (1993) 404-410.
[58] K. Gade Malmos, L.M. Blancas-Mejia, B. Weber, J. Buchner, M. Ramirez-Alvarado, H. Naiki, D. Otzen, ThT 101: a primer on the use of thioflavin T to investigate amyloid formation, Amyloid 24(1) (2017) 1-16.
[59] L.P. Jameson, N.W. Smith, S.V. Dzyuba, Dye-binding assays for evaluation of the effects of small molecule inhibitors on amyloid (Aβ) self-assembly, ACS Chem. Neurosci. 3(11) (2012) 807-819.
[60] S.A. Hudson, H. Ecroyd, T.W. Kee, J.A. Carver, The thioflavin T fluorescence assay for amyloid fibril detection can be biased by the presence of exogenous compounds, FEBS J. 276(20) (2009) 5960-5972.
[61] J. Yang, J. Guo, J. Yuan, In vitro antioxidant properties of rutin, Food Sci. Technol. 41(6) (2008) 1060-1066.
[62] For comparison the evaluation of the symmetrical analogs was made (see Table S4) using eeAChE at a concentration of 0.5U. Compounds **1'a-b**, **2'a**, **2'c**, **3'a-b** exhibited micromolar IC50 values (2-5 μM).
[63] B.M. Liederer, R.T. Borchardt, Enzymes involved in the bioconversion of ester-based prodrugs, J. Pharm. Sci. 95(6) (2006) 1177-1195.

[64] B. Furdui, O. Constantin, A. Tabacaru, R. Dinica, New bis-pyridinium diquaternary salts with antimicrobial properties, Rev. Chim 63 (2012) 667-671.
[65] D.H. Taffa, M. Kathiresan, L. Walder, B. Seelandt, M. Wark, Pore size and surface charge control in mesoporous TiO 2 using post-grafted SAMs, Phys. Chem. Chem. Phys. 12(7) (2010) 1473-1482.
[66] J. Cheung, E.N. Gary, K. Shiomi, T.L. Rosenberry, Structures of human acetylcholinesterase bound to dihydrotanshinone I and territrem B show peripheral site flexibility, ACS Med. Chem. Lett. 4(11) (2013) 1091-1096.
[67] A. Meden, D. Knez, M. Jukič, X. Brazzolotto, M. Gršič, A. Pišlar, A. Zahirović, J. Kos, F. Nachon, J. Svete, Tryptophan-derived butyrylcholinesterase inhibitors as promising leads against Alzheimer's disease, Chem. Commun. 55(26) (2019) 3765-3768.
[68] G.M. Sastry, M. Adzhigirey, T. Day, R. Annabhimoju, W. Sherman, Protein and ligand preparation: parameters, protocols, and influence on virtual screening enrichments, J. Comput. Aided Mol. Des. 27(3) (2013) 221-234.
[69] E. Harder, W. Damm, J. Maple, C. Wu, M. Reboul, J.Y. Xiang, L. Wang, D. Lupyan, M.K. Dahlgren, J.L. Knight, OPLS3: a force field providing broad coverage of drug-like small molecules and proteins, J. Chem. Theory Comput. 12(1) (2016) 281-296.
[70] H. Li, A.D. Robertson, J.H. Jensen, Very fast empirical prediction and rationalization of protein pKa values, Proteins 61(4) (2005) 704-721.
[71] J.L. Banks, H.S. Beard, Y. Cao, A.E. Cho, W. Damm, R. Farid, A.K. Felts, T.A. Halgren, D.T. Mainz, J.R. Maple, Integrated modeling program, applied chemical theory (IMPACT), J. Comput. Chem. 26(16) (2005) 1752-1780.
[72] LigPrep, LigPrep version 3.5 Schrödinger, LLC, New York, NY, 2015. 2015.
[73] Epik, Epik version 4.2 Schrödinger, LLC, New York, NY, 2017. 2017.
[74] R.A. Friesner, J.L. Banks, R.B. Murphy, T.A. Halgren, J.J. Klicic, D.T. Mainz, M.P. Repasky, E.H. Knoll, M. Shelley, J.K. Perry, Glide: a new approach for rapid, accurate docking and scoring. 1. Method and assessment of docking accuracy, J. Med. Chem. 47(7) (2004) 1739-1749.
[75] Glide, Glide version 7.7, Schrödinger, LLC, New York, NY, 2017. 2017.
[76] A. Hameed, S.T. Zehra, S.J. Shah, K.M. Khan, R.D. Alharthy, N. Furtmann, J. Bajorath, M.N. Tahir, J. Iqbal, Syntheses, cholinesterases inhibition, and molecular docking studies of Pyrido [2, 3-b] pyrazine derivatives, Chem. Biol. Drug Des. 86(5) (2015) 1115-1120.